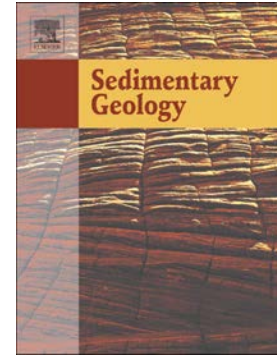


Journal Pre-proof

Characteristics and emplacement mechanisms of the Coranzulí ignimbrites (Central Andes)

Silvina Guzmán, Domenico M. Doronzo, Joan Martí, Raúl Seggiaro



PII: S0037-0738(20)30114-7

DOI: <https://doi.org/10.1016/j.sedgeo.2020.105699>

Reference: SEDGEO 105699

To appear in: *Sedimentary Geology*

Received date: 17 March 2020

Revised date: 20 May 2020

Accepted date: 21 May 2020

Please cite this article as: S. Guzmán, D.M. Doronzo, J. Martí, et al., Characteristics and emplacement mechanisms of the Coranzulí ignimbrites (Central Andes), *Sedimentary Geology* (2020), <https://doi.org/10.1016/j.sedgeo.2020.105699>

This is a PDF file of an article that has undergone enhancements after acceptance, such as the addition of a cover page and metadata, and formatting for readability, but it is not yet the definitive version of record. This version will undergo additional copyediting, typesetting and review before it is published in its final form, but we are providing this version to give early visibility of the article. Please note that, during the production process, errors may be discovered which could affect the content, and all legal disclaimers that apply to the journal pertain.

© 2020 Published by Elsevier.

Characteristics and emplacement mechanisms of the Coranzulí ignimbrites (Central Andes)Silvina Guzmán^{a,*}, Domenico M. Doronzo^b, Joan Martí^b, Raúl Seggiaro^a

^a Instituto de Bio y Geociencias del NOA (IBIGEO), UNSa, CONICET, 9 de Julio 14, 4405, Rosario de Lerma, Salta, Argentina.

^b Instituto de Ciencias de la Tierra Jaume Almera, ICTJA-CSIC, Lluís Solé i Sabarís s/n, 08028, Barcelona, Spain.

* Corresponding author: sguzman@conicet.gov.ar

Abstract

We present a detailed stratigraphy of the Coranzulí caldera-forming deposits. This caldera, located in the Altiplano-Puna Volcanic Complex (Central Andes), generated four ignimbrite deposits with similar field characteristics and facies that differ from each other in, above all, the nature of the lithic fragments they contain. Three different lithofacies (fine-grained cross-stratified facies, massive lithic breccia facies and massive ignimbrite facies) are found in all the ignimbrite deposits, which occasionally also contain a lenticular lithic-rich facies and/or a pumice-rich facies. These field characteristics and, in particular, local deposit thicknesses were used to develop a theoretical model of the dynamics and emplacement mode of the Coranzulí pyroclastic flows. Our results show that these ignimbrites were emplaced by dense pyroclastic density currents subjected to high accumulation rates and velocities, thereby indicating rapid *en masse* emplacement that was also influenced by local paleotopography as deduced from facies analysis.

Keywords: Coranzulí; Central Andes; Puna; crystal-rich ignimbrites; pyroclastic density current; Altiplano-Puna Volcanic Complex

1. Introduction

In the Altiplano-Puna Volcanic Complex (APVC; de Silva, 1989) within the Altiplano-Puna plateau large-volume explosive volcanism took place just prior to the late Miocene (Fig. 1). The

APVC (latitude 21–24°S, the Andes) produced more than 15,000 km³ of crystal-rich dacitic ignimbrites (e.g., de Silva et al., 2015) originating mostly from calderas. The intense volcanism of this area has been related to the existence of a low-velocity zone at mid-crustal levels known as the Altiplano-Puna Magma Body (e.g., Chmielowski et al., 1999).

The APVC contains at least eight calderas but the sources of many of its ignimbrite units are still unknown or buried, as is the case of the Abra Granada Ignimbrite (Caffe et al., 2008). The caldera complexes in the APVC (Fig. 1) with the greatest volumes (800-2500 km³) are La Pacana, Cerro Guacha I, Cerro Guacha II, Pastos Grandes, Kapina and Vilama (de Silva, 1989; Lindsay et al., 2001a; Soler et al., 2007; Salisbury et al., 2011; Iriarte, 2012; Grocke et al., 2017). The calderas of Cerro Panizos and Coranzulí (each about 650 km³ and 6.5-7 Ma) to the east have slightly smaller volumes and are peraluminous (Seggiaro et al., 1987, 2019; Ort, 1993).

Studies of the calderas in the APVC have to date mainly focused on their petrologic characteristics, chronology, volume estimations, the definition of their rims and structural controls, as well as the type of collapses (e.g., de Silva, 1989; Seggiaro, 1994; Ort et al., 1996; Lindsay et al., 2001a,b; Soler et al., 2007; Salisbury et al., 2011; Grocke et al., 2017; Seggiaro et al., 2019). Consequently, less attention has been paid to their stratigraphy and the modes of emplacement and deposition of the caldera-forming products, although a few studies of these calderas to varying degrees of detail do exist (e.g., Seggiaro et al., 1987; Ort, 1993; Lindsay et al., 2001a; Soler et al., 2007).

To further knowledge of the APVC ignimbrite deposits and characterise the emplacement and depositional mechanisms of these large-volume ignimbrites, we concentrated our study on the caldera-forming products originating from the Coranzulí caldera (Seggiaro et al., 1987, 2019). Our aim was to develop a theoretical model of the dynamics of the Coranzulí pyroclastic flows that furthers our knowledge of the behaviour of such large pyroclastic density currents (PDCs) and their depositional mechanisms.

Pyroclastic density currents and their deposits are generally studied using a number of different approaches (fieldwork, experimental and numerical studies) and with a variety of objectives in mind (emplacement and hazard) (Roche et al., 2013; Sulpizio et al., 2014; Neri et al., 2015; Dufek, 2016). In particular, dense PDCs emplacing ignimbrites have been studied by integrating theoretical,

stratigraphic, sedimentological, petrological, paleomagnetic and, more recently, experimental work (e.g., Sparks et al., 1978; Cas and Wright, 1987; Druitt, 1998; Branney and Kokelaar, 2002; Ort et al., 2013; Rowley et al., 2014; Roche, 2015). It is thought that dense PDCs emplacing ignimbrites are thermally conservative flows (McClelland et al., 2004; Lesti et al., 2011; Cas et al., 2011; Sulpizio et al., 2014; Giordano and Doronzo, 2017; Platzman et al., 2020). They can move whilst retaining temperature for several kilometres under the action of sustained pyroclastic fountaining with high mass eruption rates (MERs) during caldera collapse (Martí et al., 2009; Cas et al., 2011; Willcock et al., 2013; Roche et al., 2016; Trolese et al., 2017) or under the action of flow channelization (Doronzo et al., 2016; Martí et al., 2017, 2019; Pensa et al., 2019).

Our current understanding of the emplacement mechanisms of thermally conservative flows to form ignimbrites is still not fully clear due to four principal physical complexities: (i) the transmission of inertia from a low pyroclastic fountain to a dense PDC; (ii) the time-dependent evolution of pore pressure within the dense PDC; (iii) the size of the dense PDC (erupted volume versus areal extent of the PDC); and (iv) the emplacement mechanisms and temperature retention of ignimbrites (McClelland et al., 2004; Lesti et al., 2011; Cas et al., 2011; Doronzo, 2012; Roche, 2012; Roche et al., 2016; Sulpizio et al., 2014; Dufek, 2016; Dellino et al., 2019).

In order to accomplish such objective, we used previous (Seggiaro et al., 1987, 2019) and new field data of the four ignimbrite units that were emplaced during the formation of the Coranzulí Caldera, mainly concentrating on their lithological and sedimentological characteristics, as well as their stratigraphic relationships and facies variations. Using this information, we present here a theoretical depositional model for these deposits aimed at simplifying the above-mentioned complexities. This model follows reverse engineering and inverts the deposit thicknesses to calculate accumulation rates and velocities, which can be combined with field data to interpret flow emplacement, local inertia loss and interaction with topography. The accumulation rates of a pyroclastic flow deposit or, in general, of a sedimentary deposit are probably the best parameter for denoting the transition from flow to deposit given the need for a framework in which flow structure and deposit structure are the same (e.g., Roche, 2015). Hence, we kept the model as simple as possible and closely linked to field characteristics.

2. Geological setting of the Coranzulí caldera

The Coranzulí Caldera (Fig. 2) lies on the Altiplano-Puna Plateau, within the Central Andes Volcanic Zone (18-28°S segment of the Andes) (e.g., Harmon et al., 1984; Stern, 2004). It is located in at ca. 140 km from the present volcanic arc, in the back-arc region. The present-day uplifted topography of the Altiplano-Puna Plateau has been attributed to tectonic shortening induced by the subducting Nazca Plate and, also to magmatic addition (e.g., Isacks, 1988; Allmendinger and Gubbels, 1996; Kay et al., 1999; Oncken et al., 2006).

The Altiplano-Puna Plateau is structurally controlled by several sets of fault systems oriented N-S to NNE-SSW, NW-SE and NE-SW (Salfity, 1985; Riller and Oncken, 2003) and the volcanic centres they contain are aligned along these fault systems (Mon, 1979; Salfity, 1985; Marrett and Emerman, 1992; Riller et al., 2001; Richards and Villeneuve, 2002; Trumbull et al., 2006; Guzmán et al., 2014; Tibaldi et al., 2017). This is the case of the Coranzulí Caldera, which is located at the intersection of N-S, NW-SE and NE-SW fault systems (Seggiaro et al., 2014, 2019).

The Coranzulí Caldera (23° 00'S- 66° 15' W) is located in the Northern Puna (ca. 24–21.5 °S). Its basement consists of Paleozoic and Mesozoic granitoids and marine Ordovician rocks interbedded with volcanic and subvolcanic successions (Coira, 1973). Although no high-grade metamorphic pre-Ordovician outcrops exist in the Northern Puna, the presence of accessory lithic fragments of sillimanitic gneisses within the Coranzulí ignimbrites points to the presence of such a basement beneath the Ordovician sediments (Seggiaro, 1994). The pre-caldera sedimentary successions are composed of Cretaceous syn-rift and Paleogene post-rift deposits belonging to carbonatic and clastic deposits of the Salta Group and of Eocene–Miocene volcano-sedimentary deposits (See Fig. 2 in Seggiaro et al., 2019).

Pre-caldera Cenozoic volcanic activity in the Coranzulí area is represented by sandstones, pyroclastic successions and reworked volcanic material from the Middle Miocene (Seggiaro and Aniel, 1989). To the east of Coranzulí Caldera there are deposits of 7.2–8.4 Ma belonging to the Rachaite stratovolcano of andesitic–dacitic composition (Coira et al., 1993; Kay et al., 2010, and

references therein). To the southwest outcrops the Morro Grande Ignimbrite, consisting of massive and brecciated pyroclastic deposits of similar composition to those of the Coranzulí ignimbrites (López et al., 2016) covered by lacustrine deposits interbedded with massive and stratified pyroclastic deposits of 6.99 ± 0.18 Ma (Alonso, 1986). The Coranzulí ignimbrites overlie these successions (see Fig. 2 in Seggiaro et al., 2019).

3. Methodology

In addition to the previous stratigraphic data available on the Coranzulí ignimbrites, we constructed 20 new stratigraphic logs chosen on the basis of their accessibility, quality of exposure and degree of preservation (Fig. 3). In each stratigraphic log we recorded lithological and sedimentological data, including component analysis at macroscopic and microscopic scales, grain-size estimates for pumices and lithics, characterisations of basal and top contacts for each ignimbrite unit, and the thickness of each deposit. Previous and new stratigraphic data were combined in order to establish the stratigraphic correlations and facies variations of these deposits. We also measured the five largest pumice and lithic fragments (minimum and most frequent sizes) in each ignimbrite unit, as well as the maximum and minimum axes of pumice/fiamme to determine their aspect ratios. Other standard descriptions such as colour, induration degree, size of the matrix and the recognition of textures and fabrics were also noted.

4. Results

As it was already indicated by Seggiaro et al. (1987, 2019), the stratigraphic succession of the Coranzulí Caldera is composed of four different ignimbrite units. Seggiaro et al. (2019) suggested that these ignimbrites derived from four different PDCs each of which originated from a specific sector of the ring fault at a particular stage of the caldera collapse process. Our field revision confirms this stratigraphy and the fact that each ignimbrite units was emplaced from a different sector of the caldera.

The base of each ignimbrite is marked by lithic breccias at proximal distances (<5 km), while at medial distances from the caldera (5–15 km) contacts are identified by fine-grained ash layers.

However, in some outcrops the contact between ignimbrites is not that evident and they can be only distinguished by the nature and proportion of the lithic fragments they contain. The contacts between the ignimbrites can be erosional or gradational depending on the observation point, and internally they may show variations in grain size and the percentage of juvenile and lithic components, and variations in primary bedforms. All the ignimbrite units exhibit the same types of facies, e.g., fine-grained cross-stratified facies, massive lithic breccia facies and massive ignimbrite facies, which form the main body of the deposits; occasionally, they may also contain a lenticular lithic-rich facies and/or a pumice-rich facies. The characteristics of each facies are very similar in each ignimbrite unit despite certain differences in the nature of the lithic fragments, the size and degree of flattening of the pumice clasts, the degree of welding and the thickness of each one.

Near the northern edge of the caldera rim the base of the unexposed pre-caldera deposits consists of a ~10-m-thick massive indurated monolithologic breccia (Fig. 4a, b) with a matrix of fine ash containing 50–70% volume of subangular lithic fragments of dacitic lavas ranging in size up to 30–40 cm in diameter (Fig 4b). This massive and monolithologic volcanic breccia contains no pumice but does contain some vitrophyres with perlitic alteration.

4.1 Ignimbrite unit 1

This ignimbrite flow unit was emplaced north- and northwestwards but only towards the north of the caldera the base of this unit is visible. The average thickness of the ignimbrite is 50 m and the flows that fed this ignimbrite travelled for at least 28 km from the caldera rim.

The base of this unit is formed by a 4–8 m-thick, yellow–greenish fine-grained cross-stratified facies, which overlies the pre-caldera monolithologic volcanic breccia (see log 1 in Fig. 3a). Its internal structures consist of low-angle cross-stratified beds (Fig. 4 a,c,d) with internal normal grading in some sets. They are composed of quartz, plagioclase and biotite crystals and crystal fragments and rounded, well-sorted, ash pumice grains, and are rich in small lithic fragments of dacitic lavas and Ordovician metapelites, as well as in small fine lapilli (~ 0.2–0.5 cm) white pumice fragments. Some layers (up to 50-cm thick) within this succession form lenticular lithic-rich facies (lens); Figs. 3a, 4d),

in which rounded-to-subrounded lithic fragments of Ordovician pelites and dacitic lavas of up to 8 cm in diameter are concentrated in an ashy/fine lapilli matrix.

The fine-grained cross-stratified facies is covered by a massive lithic breccia facies (Figs. 3a, 4a,e) (see log 1 in Fig. 3a) with a maximum thickness of 5 m. The pumice are white, about 25 vol. %, (<5 cm in diameter), while the subangular lithic fragments (~40%) consist of dacitic lavas (up to 35–50 cm in diameter) and minor, usually very small (~0.8 cm) Ordovician metapelitic fragments (log 1 in Fig. 3a). Dense juvenile fragments (~3 vol. %) are rounded with a maximum size of 10 cm.

The massive ignimbrite facies (see log 1 in Fig 3a) is only exposed in a few places, probably because it has been covered by other younger ignimbrite units (unit 2, 3 or 4). It is grey and mostly indurated; its matrix consists of fine-to-medium ash and crystal fragments of bipyramidal quartz (translucent and pink), biotite and feldspars. Its degree of welding varies laterally and vertically, from low to moderate. The upper sections are welded and have columnar jointing. Its lithic content is low (1–3 vol. %) and decreases upwards and in distal facies and consists predominantly of dacitic lavas (log 1 in Fig. 3a) with maximum sizes of 14 cm (but usually <3 cm). The pumice content is variable, from 10–20 vol. %, and of variable sizes (usually <1 cm), white-to-yellowish or -black when they are welded, with maximum sizes of 12 cm. Dense juvenile fragments are observed in all sections at a proportion of about 1 vol. % with a diameter of <4 cm.

4.2 Ignimbrite unit 2

The base of Unit 2 is characterised by a massive lithic breccia facies lying in some areas close to the caldera (see log 2 in Fig. 3a), although in other proximal and medial sections it has a stratified indurated ash layer (fine-grained cross-stratified facies) (see Seggiaro et al., 2019). The main body of the unit corresponds to a massive ignimbrite facies showing lithic-rich lenses (lenticular lithic-rich facies) in distal locations. The maximum outflow distance is 45 km.

This ignimbrite unit (see Figs. 2, 3) was deposited radially from the caldera (Seggiaro et al., 2019) but maximum thicknesses of 200 m are present to the east (see log 5 in Fig. 3b). In proximal areas its base corresponds to a massive lithic breccia facies, highly indurated and about 5-m thick to the north of the caldera (see log 2 in Fig. 3a). Within this breccia, the pumice are white, about 15 vol.

% (<5 cm but usually small, around 0.5 cm), while the lithic fragments (~20–25 vol. %) are subangular. The main types of lithic fragments are Ordovician metapelites and quartzites (<27-cm long), whereas the dacites are subordinate. Dense juvenile fragments (~3 vol. %) reach maximum sizes of 4 cm. This massive lithic breccia facies may vary laterally (see log 3 in Fig. 3a) and develops diffuse stratification where pumice are larger (15 cm) and more abundant (30 vol. %), and lithic fragments are smaller and less abundant. At medial distances from the caldera the base of this ignimbrite unit corresponds to the fine-grained cross-stratified facies followed by the massive ignimbrite facies (see Fig. 3 in Seggiaro et al., 2019).

This massive ignimbrite facies forms the main body of the ignimbrite and is pink-to-grey in colour, with a degree of welding that varies vertically and laterally from low to high. Its matrix consists of medium-to-coarse ash and crystal fragments of pink and crystalline quartz (frequently forming bipyramidal grains), biotite and feldspars. Towards the east this ignimbrite unit is highly welded at proximal and medial distances, with fiamme aspect ratios of up to 14:1, whereas more distally (>15 km) there is only a very low degree of welding (fiamme aspect ratios of 2:1), albeit it is still indurated. The greatest amount of welding is to the north, towards the surface, and more distally, and has aspect ratios of 8:1. Pumice fragments are white-to-yellowish in colour in poorly welded sectors but form black (Fig. 5a) and pink fiamme (Fig. 5b) in welded sectors. The concentration of pumice clasts is highly variable both vertically and laterally; in proximal areas their content lies in the range 5–25 vol. % but they are usually more abundant towards the top of the succession. More distally, their content also varies greatly (5–30 vol. %). Except for the outcrops to the north, where well-defined fiamme (<16-cm long) are visible, all other distal exposures are non-welded, with white-to-yellow rounded pumice up to 10 cm in length and rich in crystal fragments. The largest pumice are found at intermediate distances from the caldera, where they reach up to 21 cm in diameter. The most common pumice size in both proximal and distal facies is 0.5–3 cm.

Lithic fragments are scarce, usually <1 vol. % but occasionally up to 7 vol. % (exceptionally they reach 25 vol. %), angular, predominantly composed of Ordovician metapelites and quartzites (see Fig. 3) and, to a much lesser extent, dacitic lava fragments. In sections to the east of the caldera there is an increase in dacitic lithic fragments towards the upper part of the deposit; however, in all cases

lithics from the Ordovician basement are the most abundant. Lithic fragments are usually small (0.5–4 cm), although fragments measuring 16–18 cm are present in distal facies and proximal upper facies. Dense juvenile fragments are observed in all sections and are about 1–3 vol. %, with sizes of up to 16.5 cm.

This lenticular lithic-rich facies is observed in distal zones and represents a transition to the massive ignimbrite facies in which it is hosted (Fig. 6a). This facies can be seen at the front of the flow unit (see log 14 in Fig. 3c) at approximately 18 km northwest of the caldera rim (see Fig. 2), where it is up to 2 m thick. The matrix is composed of coarse ash with a lithic content of about 40 vol. %, most of which consists of subangular (Fig. 6b) quartzites with a maximum clast size of 30 cm.

4.3. Ignimbrite unit 3

This unit has a basal massive lithic breccia facies to the northwest of the caldera (see Casa Blanca log, Fig. 4 in Seggiaro et al., 2019) but is composed mainly of a massive ignimbrite facies with lenticular lithic-rich facies in proximal settings and a pumice-rich facies in the uppermost and proximal part of the deposit. Its average thickness is 40 m and its most distal outcrops are 37 km from the caldera rim. The basal massive lithic breccia facies attains a maximum thickness of 6 m and consists mainly of dense co-magmatic lithic fragments (up to 80 cm in diameter) and variable amounts of Ordovician sedimentary rocks, dacitic lavas and metamorphic lithics (gneiss) (Fig. 6c). As in the previous ignimbrite units, at medial distances the base of this third ignimbrite unit corresponds to an indurated ash layer visible in the Abra Grande log (Fig. 4 in Seggiaro et al., 2019).

The massive ignimbrite facies is light-to-dark grey or -pink due to surface alteration (Fig. 6d). Welding varies from low to high, being the most welded parts located towards the top of the deposit. The ignimbrite matrix consists of medium-to-coarse ash and crystal fragments of quartz (pink and crystalline), biotite and feldspars. Pumice fragments are white to yellow and rounded in non-welded facies; on the other hand, black and pink fiamme are found in the welded facies. Pumice content is variable (10–25 vol. %) but usually high (20–25 vol. %); pumice can be up to 17 cm in diameter, although the commonest sizes are 2–3 cm. This ignimbrite is poor in lithic fragments, usually <1 vol. %, and are mainly small (0.5–2 cm), reaching a maximum size of 26 cm in diameter in proximal and

basal zones. Lithic fragments are of the same type as those found in the massive lithic breccia, although small amounts of small-sized porphyritic dacites and Cenozoic red pelites and sandstones are also present. Rounded, dense juvenile grey lithic fragments represent 1–3 vol. % and are up to 25 cm in diameter.

A massive pumice-rich ignimbrite facies can be distinguished at proximal sites (see Seggiaro et al., 2019), where up to 25 vol. % of rounded pumices are concentrated towards the upper levels of the deposit. This facies has up to 3 vol. % of dense grey juvenile fragments that are <14 cm in diameter. Pumices are white-to-yellow, crystal-rich (30–60%) and usually subrounded and small (0.5–3 cm), even though larger fragments, frequently recognised as *fiamme*, can reach 18 cm in diameter. Fragments of dense juvenile fragments are ubiquitous, subrounded, up to 25 cm in diameter, with content <1–3% in volume.

Additionally, lenticular lithic-rich facies are observed at proximal facies in transition to the massive ignimbrite facies that host them. The main lithic type in this lenticular facies is dacitic lava (see Norte de Coranzulí log Fig 4 in Seggiaro et al., 2019).

4.4. Ignimbrite unit 4

The fourth ignimbrite unit is located to the south of the caldera and travelled 18 km from the caldera rim. It has at its base a pink massive lithic breccia facies, ~ 8 m thick, that contains ~15–30 vol. % of crystal-rich white pumice; its upper portion is highly indurated. It is characterised by the presence of blocks of dacitic ignimbrites (Fig. 7h) up to 50 cm in diameter, and minor sedimentary Ordovician lithics, dacitic lavas and a few metamorphic and granitoid fragments. Dense grey juvenile fragments up to 10 cm in diameter are also visible in this facies. The breccia is overlain by the massive ignimbrite facies, which in very proximal outcrops (log 15 in Fig. 3d) near the caldera rim have an interbedded fine-grained cross-stratified facies (Figs. 7 a-c). The latter forms individual layers of less than 2 m in thickness, each interbedded with the massive ignimbrite facies, which exhibit cross (Fig. 7a) and planar (Fig. 7b) stratification and contain abundant pumice fragments and dense juvenile lithic fragments. In this facies, levels of concentrations of pumice (up to 50 vol. %) are common where the matrix presents vapour-phase alteration, probably due to the release of gases from the pumice

fragments during cooling. These layers, being originally more porous are hence more prone to vapour-phase alteration (Smith, 1960) are harder and darker than the unaltered layers (see Fig. 7d). Dense grey juvenile fragments are up to 30 cm in diameter in this succession. No other lithic fragments are present within this sequence of alternating stratified and massive facies.

The massive ignimbrite facies is grey-to-pink in colour and its matrix consists of medium grained ash and crystal fragments of quartz, biotite and feldspars. The degree of welding is variable, being greater in proximal and upper sections where columnar jointing is frequent (Figs. 7e) but only slightly welded-to-non-welded in distal outcrops. The pumice content is variable but is usually above 20 vol. %, with some concentration levels of up to 50 vol. % (pumice-rich massive ignimbrite facies; see log 17 in Fig. 3d). The pumice are white and crystal-rich and rounded-to-subrounded when the ignimbrite is non-welded (Fig. 5c) but contain grey-to-black fiamme (Fig. 5d) when welded. Although most pumices are small (1–2 cm), maximum sizes vary from 8 to 18 cm, with the largest fragments visible at medial and distal distances from the caldera rim. This facies is lithic-poor (<1%) and usually has small fragments (0.5–1 cm with maximum sizes of <4 cm) of Ordovician pelites and quartzites, dacitic lavas, metamorphic fragments and Cenozoic red pelites and dacitic ignimbrites. Dense juvenile fragments (Fig. 5c) are <3 vol. %, and are up to 30 cm in diameter in proximal facies, 25 cm in medial facies, but smaller in distal facies.

The pumice-rich massive ignimbrite facies is found in proximal and distal areas (Fig. 7g) at about 18 km from the caldera rim. Pumices represent up to 50 vol. %, vary in size (0.5–18 cm in diameter) and are embedded in a matrix of medium-to-coarse ash. This pumice-rich massive ignimbrite facies is poorly sorted and contains small amounts of lithic fragments of dacitic ignimbrite (Fig. 7f) up to 65 cm in length and dense grey juvenile fragments. They have diffuse margins that grade continuously into the enclosing massive ignimbrite. This ignimbrite is about 4 m thick but its lateral extension – probably of just a few metres – is imprecise as it only appears as eroded discontinuous outcrops.

5. Depositional model

5.1 Model design

The importance of accumulation rates and velocities is increasingly being recognised not only for volcanic deposits but also for sedimentary deposits in general (e.g., Lowe, 1988; Kneller and Branney, 1995; Girolami et al., 2010; Doronzo et al., 2012, 2017; Breard et al., 2016; Dellino et al., 2019). The theoretical model we develop here aims to estimate the accumulation rates of the Coranzulí ignimbrite deposits by inverting the field deposit thicknesses and introducing a dimensionless temperature that expresses the variation rate of temperature during emplacement. This should be regarded as a reverse engineering problem, in which the dense PDC is not directly modelled. Conceptually, we approximate the depositional system of the dense PDC as a dense single-phase flow, which supplies sediment for the growing deposit (see Legros and Martí, 2001; Roche, 2015).

The first equation of the model defines the accumulation rate A_r from the dense PDC as the rate at which the final deposit builds up from the substrate to the surface (after Doronzo et al., 2016; Giordano and Doronzo, 2017; see also Martí et al., 2019, for application to welded deposits)

$$A_r = \frac{T_{dep}}{T_p} \frac{h\rho_p}{t} \quad (\text{Eq. 1})$$

where the deposit thickness h refers to the cumulative or total deposit emplaced by various flow pulses (each one emplacing a depositional unit, i.e., lamina, massive layer), ρ_p is the average density of all the particles involved, t is the emplacement timescale, T_{dep} is the average temperature of the flow at emplacement, and T_p is the particle (weighted average of juvenile and lithic fragments) temperature. Thus, Eq. 1 contains an accumulation velocity, h/t , and a dimensionless temperature, T_{dep}/T_p . Following Sulpizio and Dellino (2008) and Doronzo and Dellino (2014), we separate the concept of ‘flow’ from that of ‘current’, which implies that various flow pulses, i.e., individual pyroclastic flows, could have sustained the currents that generated the Coranzulí ignimbrites (a time-dependent issue). We consider the deposit thickness as local as we cannot rule out the possibility that more than one current (probably from different ring-fault sectors; see Seggiaro et al., 2019) formed the final deposit by overlapping at a specific site (a space-dependent issue). Another limitation is that the deposit thickness likely represents a minimum thickness, because some erosion could have occurred in an arid region like Altiplano-Puna. This is a common issue in stratigraphy in general, particularly

when relatively old rocks are involved, and when erosion rates are difficult to assess. On the other hand, we consider the whole studied pyroclastic sequence as built up in a single eruption, which implies that the proportion between the different ignimbrite units could have not been particularly affected by erosion. For the dimensionless temperature, we consider two opposite cases: (i) $T_{dep} < T_p$, whereby the pyroclasts cool down in relation to their initial temperature (heat loss) without ever falling below the glass transition temperature (Martí et al., 1991); and (ii) $T_{dep} > T_p$, whereby the pyroclasts heat up in relation to their initial temperature (strain heating) and stay reasonably above the glass transition temperature (Robert et al., 2013). In order to take into account both thermal cases, we consider a range of T_{dep}/T_p of 0.7–1.5, which is compatible with reduced flow dilution within the dense PDC (Walker, 1972; see also Girolami et al., 2015).

The timescale of the emplacement of the ignimbrites (from substrate to surface) depends not only on the duration of the eruption but also on local depositional mechanisms affected by topography (Branney and Kokelaar, 2002; Sulpizio et al., 2014). In large volume eruptions, the substrate involved during the deposition, i.e., the paleotopography, is most of the times completely covered by the resulting deposits. This happens in our case study, so the best way to account for flow-topography interaction is to focus on the relative proportions of local deposit thicknesses (see next equation) and facies variations as a function of the accumulation rate. In these eruptions, however, paleotopography can locally affect the deposition only when inertia dominates in flow transportation (Doronzo, 2012; Roche, 2012; see discussion). At a specific site, the emplacement timescale must be shorter than the entire duration of the eruption, t_{erupt} , as there is no deposition between the onset of the eruption and the passage of the dense PDC away from the site (Rowley et al., 2014; Platzman et al., 2020). This is also valid for very proximal zones where the pyroclastic sediment is somehow laterally displaced under the action of Mass Eruption Rate (Roche, 2012; Roche et al., 2016; Giordano and Doronzo, 2017; Sweeney and Valentine, 2017; Dellino et al., 2019). In particular, we refer to t_{erupt} as the duration of pyroclastic flow phase, from generation to emplacement in a single eruption, which in our case study coincides with the entire eruption duration as for the absence of an early Plinian phase. The broad inequality $t < t_{erupt}$ will account for the complex mechanisms of deposit formation given that the onset of the emplacement from the depositional system, i.e., the decoupling of the sediment from the flow,

should be regarded as very rapid (Roche, 2012; see also Sulpizio et al., 2007; Sulpizio and Dellino, 2008; Doronzo, 2012; Breard et al., 2016; Platzman et al., 2020). For the Coranzulí eruption, we assume a range of t_{erupt} of 5–50 h, which is reasonable for a large sustained explosive eruption (Self, 2006; Costa and Martí, 2016).

The second equation calculates approximately the emplacement timescale as the product of the entire eruption and a dimensionless thickness, h_{sz}/h

$$t \approx \frac{h_{sz}}{h} t_{erupt} \quad (\text{Eq. 2})$$

A word of caution must be spent with reference to the direct application of Eq. 2. Macroscopically, we assess that the dimensionless thickness can be appropriate for scaling the eruption duration to the emplacement timescale because h is the total deposit thickness, while the shear zone thickness, h_{sz} , defines the level of upward migration, from substrate to top, of the depositional system subject to strain rate within the pyroclastic flows. The shear zone thickness can also be regarded as the thickness of the depositional unit, which for the Coranzulí ignimbrites is of the order of meters to tens-of-meters related to the massive units of the pyroclastic flow deposits (layer up to 1 m, bed > 1 m). The concept around Eq. 2 is that no deposition occurs in a site until the pyroclastic flow reaches that site, and this justifies the inequality between t and t_{erupt} . Then, each flow emplaces its own depositional unit, and the sum of the depositional units defines the total deposit at that site, and this justifies the inequality between h_{sz} and h . Considering that the temporal scale in sedimentary systems is recorded in vertical direction in the deposits, we are confident that h_{sz}/h is appropriate for capturing the deposit growth and level of upward migration at the site (through t) as the eruption progresses and feeds the dense currents at the vent (through t_{erupt}). Generally, $h_{sz} \ll h$ (Doronzo and Dellino, 2013; Robert et al., 2013; Martí et al., 2017; Dellino et al., 2019), from which we can derive the inequality $t \ll t_{erupt}$, which means that the final deposit at a specific site can form in a time that is shorter than the entire eruption duration (see also Lavallée et al., 2015; Platzman et al., 2020). This is reasonable during large ignimbrite- and caldera-forming eruptions, since a substantial amount of the

sediment is deposited ahead of the site, as it spreads out from the caldera rim under the action of Mass Eruption Rate (Costa and Martí, 2016; Giordano and Doronzo, 2017).

The third equation of the model gives the accumulation rate by combining Eq. 2 and Eq. 1

$$A_r = \frac{T_{dep} h^2 \rho_p}{T_p h_{sz} t_{erupt}} \quad (\text{Eq. 3})$$

This equation enables us to conduct a parametric study of a theoretical reference scenario for the Coranzulí eruption, using the following ranges: $0.7 \leq T_{dep}/T_p \leq 1.5$, $5 \leq t_{erupt} \leq 50$ h, and $1 \leq h_{sz} \leq 2$ m. Equation 3 does not consider the eruption rate as it does not directly influence the accumulation rate for large volume eruptions. In particular, the entire eruption duration will account for the cumulative dispersion of dense PDCs during the pulsating caldera collapse event, while the shear zone thickness will account for flow-deposit interface in which the strain rate is the highest (cf., Roche, 2012; Rowley et al., 2014). We chose such ranges to keep the model as general as possible, then the described stratigraphy will constrain the application to our case study.

5.2 Model description

We first examine a reference scenario for a theoretical large explosive eruption and then compare it with the Coranzulí case study. In particular, we use as an example an eruption of several hundreds of km³ of silicic magma, with Mass Eruption Rates of 10^9 – 10^{11} kg/s, lasting from a few hours to a few days (Costa and Martí, 2016). Within this timeframe, there is time for the emplacement of ignimbrites under the inequality $t \ll t_{erupt}$ (Lavallée et al., 2015; Platzman et al., 2020). We also assume a single deposit thickness of 100 m and a particle density of 2000 kg/m³. In Fig. 8, the accumulation rate is plotted as a function of the dimensionless temperature in a range $h_{sz} \cdot t_{erupt}$ of 5–100 m·h. These two values correspond to the extreme cases $h_{sz}(\text{min}) \cdot t_{erupt}(\text{min})$ and $h_{sz}(\text{max}) \cdot t_{erupt}(\text{max})$, respectively, while all possible combinations lie in between these extremes (shaded area in Fig. 8).

The physical meaning of Fig. 8 is that the shorter the eruption, the faster the formation of the deposit. The slowest scenario gives an accumulation velocity of 28 mm/s and a minimum accumulation rate of 39.2 kg/m² s, while the fastest gives an accumulation velocity of 550 mm/s and a

minimum accumulation rate of $770 \text{ kg/m}^2 \text{ s}$. These values give broad ranges for these two quantities due to the variability in the duration of the eruption and indicate that (i) accumulation velocities of $\geq 28 \text{ mm/s}$ are typical of dense PDCs emplacing ignimbrites by rapid progressive aggradation; and (ii) accumulation velocities of 550 mm/s are typical of dense PDCs emplacing ignimbrites by rapid *en masse* emplacement. Such orders of magnitude have been reported in large-scale laboratory experiments with dense PDCs (e.g., Roche, 2012; Rowley et al., 2014; Girolami et al., 2015; Breard et al., 2016; Breard and Lube, 2017; Sulpizio et al., 2016). Thus, the dominant mode of emplacement of ignimbrites will be either rapid progressive aggradation or rapid *en masse* emplacement, depending on the eruption timescale. Nonetheless, a combination of these two modes will probably occur in any single large eruption, as the accumulation rate changes over space (due to local topography) and time (due to the pulsating event).

Finally, the intercept $T_{dep}/T_p = 1$ in Fig. 8 separates the fields characterised by heat loss ($T_{dep}/T_p < 1$) and strain heating ($T_{dep}/T_p > 1$). The physical meaning of the relationship between the accumulation rate and the dimensionless temperature is that the faster the accumulation, the more thermally conservative the deposit (cf., Michol et al., 2008; Lavallée et al., 2015; Doronzo et al., 2016; Giordano and Doronzo, 2017; Trolese et al., 2017; Martí et al., 2019). For example, welded ignimbrites will form at relatively high accumulation rates, whereas lava-like lithofacies will occur at extremely high accumulation rates ($\sim 1000 \text{ kg/m}^2 \text{ s}$). We suspect that the latter case is most likely to occur in intra-caldera settings under highly sustained pyroclastic fountaining.

6. Discussion

6.1. Deposits and flow characteristics

The Coranzulí Caldera formed about 6.6 Ma ago and generated 650 km^3 of crystal-rich dacite ignimbrite deposits, which are distributed to the north, northwest, east and south (Fig. 2) over an area of 2050 km^2 (Seggiaro et al., 1987, 2019). This caldera-forming eruption has recently been interpreted as a pulsating boiling-over event in which the caldera collapse developed immediately after the onset of the eruption, favoured by a transtensive tectonic system (Seggiaro et al., 2019). Under these

conditions, caldera collapse was not homogeneous, occurring along different sectors of the ring fault as subsidence progressed, as indicated by the presence of the massive lithic breccia facies, which can be interpreted as co-ignimbrite lag breccias (Seggiaro et al., 1987) with different lithic components at the base of each ignimbrite unit.

In figure 9 we present an integrated interpretation of the facies architecture of Coranzulí ignimbrites based on the sum of new and published (Seggiaro et al., 2019, and references therein) stratigraphic logs. This schematic representation highlights the vertical and lateral facies variations of Coranzulí ignimbrites discussed below. The distribution of the ignimbrite units in different directions from the caldera rim are related with the interpreted caldera collapse dynamics by Seggiaro et al (2019).

The absence of Plinian fallout deposits, as has been observed in many other calderas in the Central Andes (e.g., Cerro Galán: Sparks et al., 1985, Cas et al., 2011; Vilama: Soler et al., 2007; Aguas Calientes: Petrinovic et al., 2010; Luingo: Guzmán and Petrinovic, 2010), and the relatively low depletion of fines through elutriation indicate that the flows that fed the pyroclastic currents were mostly concentrated and not much thicker than their resulting deposits (Seggiaro et al., 2019). The presence of the fine-grained cross-stratified facies in some proximal settings (Fig. 9) can be interpreted as the result of locally diluted flows, dominated by traction during their emplacement (e.g., ignimbrite unit 1), which could be the result of their deposition on a steep slope after flow-topography interaction (e.g., Branney and Kokelaar, 2002; Sulpizio et al., 2014; Giordano and Doronzo, 2017). It is even possible to find these same lithofacies at significant distances from source, depending on the morphology of the substrate, and wherever the flows were not directly affected by the Mass Eruption Rate but, instead, influenced mainly by their own inertia (Roche, 2015; Giordano and Doronzo, 2017). These are the main physical conditions to have flow-topography interaction as effective in large volume pyroclastic flows and associated deposits. It is to remark once again that in our case study the whole pyroclastic sequence covers the paleotopography in most outcrops. In the fine-grained cross-stratified facies of ignimbrite unit 1 to the north of the caldera some lenticular lithic-rich facies were identified in the stratified succession. As these deposits are very proximal, we believe that they were derived from drag forces that picked up lithics from the substrate, which were then locally deposited

by granular jumps (cf., Martí et al., 2019). This hypothesis is supported by the character and composition of the fragments (rounded to subrounded fragments of dacites and metapelites and quartzites from the Ordovician basement). However, we cannot exclude that some lithics could also derive from erosion of the caldera wall due to the caldera collapse and successive caldera enlargement. These deposits, which are very localised, may correspond to an initial explosive phase that locally preceded the opening of the ring fault. This is suggested by the fact that in ignimbrite unit 1 this deposit grades transitionally into the massive lithic breccia facies rich in dacitic lava lithics, which can be interpreted as a co-ignimbritic lithic lag breccia that gradually changes into the massive ignimbrite facies. The massive ignimbrite can be interpreted as having formed under flow boundary zones that are transitional between granular and fluid-escape-dominated flows.

The massive lithic breccia facies at their base in proximal zones was interpreted by Seggiaro et al (2019) as a co-ignimbritic lag breccia representing the opening (or widening) of conduits within the area of the caldera rim. In some logs (see log 1 and 15 in Fig. 3a,d, 9c) the base of these ignimbrite units has a fine-grained cross-stratified facies that is the result of traction-dominated parental flows, probably after flow-topography interaction (inertia condition; Doronzo, 2012; Roche, 2012). As with Ignimbrite unit 1, the massive ignimbrite facies in units 2, 3 and 4 were formed under flow boundary zones that were transitional between granular and fluid-escape-dominated flows.

In Ignimbrite unit 2, of note is the lenticular lithic-rich facies up to 2 m thick found at about 18 km to the northwest of the caldera rim (Fig. 9c), which has transitional contacts with the massive ignimbrite facies in which it is enclosed; blocks are up to 30 cm in diameter. Similar lithic-rich lenses have been described from other ignimbrites (e.g., Le Penec et al., 1994). Recently, Roche (2015) performed experimental analyses in an attempt to understand the conditions required for the formation of this facies tens of kilometres from its source. This author's experiments show that clast sizes entrained by dilute currents reach up to 15 cm in diameter but that entrainment by a PDC consisting of a dense basal flow with high interstitial gas pore pressure can uplift even bigger substrate particles – due to the upward pressure gradient at the flow-substrate interface – and then transport and deposit them in the basal deposit of the flow by granular jumps (cf., Martí et al., 2019). Roche (2015) derived a velocity of the parent dense PDCs of up to ~25–30 m/s for ignimbrites with lithics up to 2 m. We

applied Roche's (2015) equation 8 using the features of the largest fragment in a lenticular lithic-rich facies at a flow front. We considered a density of 2700 kg/m^3 for a quartzite lithic fragment of ellipsoidal shape with a minor axis of 0.25 cm, and assumed a current bulk density of 1400 kg/m^3 and a density of the interstitial fluid of 1 kg/m^3 . We obtained a velocity of 7.43 m/s for the PDCs of Coranzulí, which is similar to those of the Galán ignimbrites ($\sim 8\text{--}10 \text{ m/s}$) (Roche, 2015, and references therein). This is further evidence of the mobility of the flows that formed the Coranzulí ignimbrites and implies that they were highly concentrated PDCs that were moving at relatively low velocities.

In similar way, it is worth mentioning the presence in some ignimbrite units of a pumice-rich massive ignimbrite facies (see log 17 in Fig. 3d). This is thought to have formed at a flow boundary zone dominated by granular flow, a theory backed by the massive character of the ignimbrite, the absence of elutriation pipes, and the relatively similar crystal contents within the pumices and matrix. Hence, the pumice may have segregated as flotsam because of their inability to percolate down into the granular flow (e.g., Branney and Kokelaar, 2002). They may have travelled long distances as a result of this overpassing (see distal facies of ignimbrite unit 4 in Fig. 3d, 9d). However, the presence of some lithics up to 65 cm in length in this sequence (see Fig. 7f) and the poor sorting of the pumice (Fig. 7g) may indicate that these pumice were deposited as flotsam and were immediately remobilised by a subsequent, more concentrated part of the flow capable of transporting large blocks. These blocks, once deposited, settled down in the recently sedimented pumice-rich layer. The above-mentioned blocks of ignimbrites are indistinguishable in composition from those of the Coranzulí ignimbrites, which thus may indicate that these fragments were part of an ignimbrite that is compositionally similar to and slightly older than those from Coranzulí. Evidence for the occurrence of older ignimbrites of similar compositions to those from Coranzulí can be found nearby, as for example in the Morro Grande ignimbrites (López et al., 2016).

6.2. Model application

To apply this model to the Coranzulí ignimbrites we used our field measurements of the local deposit thicknesses – we chose not to consider a single thickness as representative of the whole

deposit (reference scenario) – to calculate site-by-site the corresponding accumulation rates. From each measurement, we also calculated the accumulation velocities and the emplacement timescales (Table 1). The results shown in Fig. 8 refer to a theoretical large explosive eruption with uniform emplacement (single deposit thickness). In Table 1, however, we highlight the spatial variability in the emplacement of the Coranzulí deposits (local thicknesses). It is to mention, as explained in the formulation of the model, that the local deposit thicknesses are to be considered as minimum thicknesses, as we cannot exclude that erosion occurred over the 6.6 Ma, which is a general issue for volcanic successions in explosive volcanism.

When considering the general characteristics of the Coranzulí ignimbrites, we took into account two important factors: (i) each local measurement corresponds to the total thickness of the deposit on a site-by-site basis as it was impossible to know precisely whether or not all dense currents (each one giving rise to an ignimbrite unit) reached all the sites during the pulsating caldera collapse event; and (ii) given that the Coranzulí deposits are mostly moderately welded, we first excluded strain heating (Fig. 8) and then opted for $T_{dep}/T_p = 0.7$, which is still a thermally conservative case. The first factor gives qualitative results, with the limitation that the accumulation rates change over time. The second factor relates to the textural characteristics of the deposits, which are far from being strongly welded, high-grade or lava-like ignimbrites (cf., Wilson and Hildreth, 2003; Quane and Russell, 2005; Michol et al., 2008; Robert et al., 2013; Pacheco-Hoyos et al., 2018).

Table 1 reveals that the thicker the deposit, the faster its accumulation. The slower cases give accumulation velocities of <10 mm/s and accumulation rates of <12 kg/m² s. These cases are the minority and, except for log 10, correspond to the most distal sites of the Coranzulí deposits. By contrast, the faster cases have accumulation velocities of >20 mm/s and accumulation rates of >28 kg/m² s. These cases are the majority and correspond to the proximal and medial-to-distal sites of the ignimbrite deposits. Each case defines a broad range of the two calculated quantities due to the variability of the duration of the entire eruption. These ranges vary due to variability in the thicknesses of the local deposits, which shows that, while at some sites the formation of the Coranzulí ignimbrites was slow, at others it was swift (maximum accumulation velocities >350 mm/s). In particular,

minimum accumulation velocities of >50 mm/s for logs 5 and 9 indicate that the local accumulation was rapid.

The Coranzulí ignimbrite sequence is very thick and conceals the paleotopography and so the application of the depositional model only allows us to infer general flow dynamics: (i) dense currents led to the Coranzulí ignimbrites piling up over time during a sustained large explosive eruption, i.e., for the duration of the whole eruption (caldera scale); and (ii) each pyroclastic flow sustaining a current emplaced the various depositional units by rapid accumulation, and the facies variations in the deposits were likely also dependent on local paleotopography (cf., Sparks et al., 1973; Doronzo, 2012; Roche, 2012; Sulpizio and Dellino, 2008; Martí et al., 2017, 2019).

Our theoretical model of long-lived, large-volume dense PDCs emplacing the Coranzulí ignimbrites gives a threshold for the accumulation rate of ≥ 39.2 kg/m² s. Such an order of magnitude is found in large-scale laboratory experiments carried out on dense PDCs (Roche, 2012; Girolami et al., 2015; Breard et al., 2016). On the other hand, a threshold for the accumulation rate of < 5 kg/m² s has been derived from recent 3D numerical simulations and experiments on short-lived, small-volume PDCs (Doronzo et al., 2017; Dellino et al., 2019). These two accumulation rates, which diverge in orders of magnitude, are thought to be responsible for the emplacement of massive versus laminated deposits at local scales, respectively (Doronzo et al., 2017; Giordano and Doronzo, 2017; Dellino et al., 2019). Conversely, the eruptive conditions for the formation of a PDC are important at a volcano scale (Doronzo et al., 2016; Sweeney and Valentine, 2017). In particular, low values for the accumulation rates will correspond to small- to intermediate-volume dilute PDCs, which lose a substantial amount of solid load in proximal areas due to short-lived, vertical column collapse and ground impact (Doronzo et al., 2017; Dellino et al., 2019; Navarrete et al., 2020).

The resulting goal after applying the theoretical model is to relate the emplacement mechanisms to the eruptive mechanisms at Coranzulí. In this sense, our model is consistent with a sustained large-volume explosive eruption, in which dense PDCs formed as a consequence of low, dense pyroclastic fountaining with retained temperature and reduced air entrainment (Sparks and Wilson, 1976; Bursik and Woods, 1996; Guzmán and Petrinovic, 2010; Petrinovic et al., 2010; Dufek, 2016; Pacheco-Hoyos et al., 2018; Dellino et al., 2019). Other similar caldera-forming events show

that the application of the model to the Coranzulí case study is consistent with cases such as Cerro Galán (Cas et al., 2011), Vilama (Soler et al., 2007), Aguas Calientes (Petrinovic et al., 2010) and La Pacana (Lindsay et al., 2001a), which all have similar field characteristics. The absence of Plinian fallout deposits preceding the emplacement of the four ignimbrite units – and the very low elutriation of fine-grained particles – support this view (Walker, 1972) and argue against the existence of a high-rising then collapsing vertical column with associated dilute PDCs, as occurs more frequently in small-volume eruptions (cf., Sulpizio et al., 2014; Roche, 2015; Navarrete et al., 2020). The general conceptual model that derives from the Coranzulí case study is thus that of dense PDCs emplacing large ignimbrites during a sustained large-volume eruption (Cas et al., 2011; Ort et al., 2013; Willcock et al., 2013; Sulpizio et al., 2014; Costa and Martí, 2016; Roche et al., 2016; Trolese et al., 2017; Pacheco-Hoyos et al., 2018) dominated by forced convection (Doronzo, 2012; Giordano and Doronzo, 2017), in which local topography enhances flow inertia and deposit facies variation in correspondence of the fine-grained cross-stratified facies (Doronzo, 2012; Roche, 2012).

Conclusions

The Coranzulí Caldera (23°00'S-66° 15'W) generated four thick, crystal-rich (30–60%) ignimbrite units with varying pumice (usually >20%) and lithic clast (from <7% to >25%) content.

The caldera eruption occurred in different pulses in different sectors of the ring fault and generated very low dense eruption columns with little air entrainment that collapsed almost immediately and continuously. This was then succeeded by concentrated PDCs that travelled at relatively low velocities (less than tens of m/s). These PDCs were dominated by granular-to- (less frequently) fluid-escape-dominated flow boundary zones that generated the massive ignimbrite facies. Some minor pauses in the eruption are revealed by the presence of sudden contacts between lithofacies and by the presence of small co-ignimbritic ash-cloud surges such as those identified by Seggiaro et al. (2019). Throughout each of the ignimbrite units, different lithofacies including co-ignimbritic lag

breccias, fine-grained stratified facies, and prominent massive lithofacies are visible, thereby indicating the presence of different mechanisms of transport and deposition for these currents.

Our theoretical model allows us to explain these very different types of flow behaviour. The fine-grained proximal lithofacies was formed by locally diluted flows, with flow boundary zones dominated by traction during their deposition on a steep slope. These stratified lithofacies are the minority and correspond to flow emplacements under relatively low accumulation rates, as derived from the theoretical model applied to the Coranzulí case study. By contrast, the massive lithofacies corresponds to flow emplacement with high accumulation rates, when pyroclastic flows were still far travelling under the effects of Mass Eruption Rate during the sustained eruption. In particular, some alternation of stratified and massive thin sets of deposits in proximal settings probably reflects oscillatory flow-boundary conditions, varying from a fluid-escape-/granular-flow-dominated flow boundary zone to a traction-flow-dominated boundary zone. These conditions can be related to the unsteadiness associated with dynamical changes in topography, which in turn are probably related to the mechanisms of the syn-eruptive subsidence and the widening of the caldera rim. In other words, the topography was changing during the eruption itself. On the other hand, lithic-rich lenses were formed by the uplift of substrate blocks by a dense basal flow with high interstitial gas pore pressure, which was able to transport and deposit these blocks on the basal deposit of the flow.

The depositional model derived from the study of the Coranzulí ignimbritic succession, which is particularly thick and conceals the paleotopography, can also be applied to infer general flow dynamics from other similar large-volume, crystal-rich, caldera-forming ignimbrites in the same area. These large ignimbrites were, in the majority, emplaced by pyroclastic flows by rapid accumulation in a long-lived eruption dominated by forced convection, while their internal facies variations were, in the minority, influenced by local paleotopography.

Acknowledgements

This work was supported by Agencia Nacional de Promoción Científica y Técnica (PICT-2012-419; PICT-2017-2798; PICT-2017-1928) and the Consejo Nacional de Investigaciones Científicas y Técnicas (PUE 2016-2021), Argentina. SG is grateful to Elena López, Albano Floridia and Emanuel

Ramos for their assistance in the field and Valmir da Silva Souza for the helpful discussions. JM is supported by the Spanish Grant CGL2017-84901-C2-1. We thank the constructive reviews of two anonymous referees, and the editor, Jasper Knight. English text was reviewed and corrected by Michael Lockwood.

References

- Allmendinger, R., Gubbels, T., 1996. Pure and simple shear plateau uplift, Altiplano–Puna, Argentina and Bolivia. *Tectonophysics* 259, 1–13.
- Alonso, R., 1986. Ocurrencia, posición estratigráfica y génesis de los depósitos de boratos de la Puna Argentina (Ph.D. thesis). Universidad Nacional de Salta, Argentina.
- Branney, M.J., Kokelaar, B.P., 2002. Pyroclastic density currents and the sedimentation of ignimbrites: Geological Society of London Memoirs 27, London.
- Breard, E.C.P., Lube, G., 2017. Inside pyroclastic density currents—Uncovering the enigmatic flow structure and transport behaviour in large-scale experiments. *Earth and Planetary Science Letters* 458, 22–36.
- Breard, E.C.P., Lube, G., Jones, J.R., Dufek, J., Cronin, S.J., Valentine, G.A., Moebis, A., 2016. Coupling of turbulent and non-turbulent flow regimes within pyroclastic density currents. *Nature Geoscience* 9, 767–771.
- Bursik, M.I., Woods, A.W., 1996. The dynamics and thermodynamics of large ash flows. *Bulletin of Volcanology* 58, 175–193.
- Cas, R.A.F., Wright, J.V., 1987. *Volcanic Successions Modern and Ancient: a geological approach to processes, products and successions*. Allen & Unwin, London.
- Cas, R.A.F., Wright, H.M.N., Folkes, C.B., Lesti, C., Porreca, M., Giordano, G., Viramonte, J.G., 2011. The flow dynamics of an extremely large volume pyroclastic flow, the 2.08-Ma Cerro Galán Ignimbrite, NW Argentina, and comparison with other flow types: *Bulletin of Volcanology* 73, 1583–1609.

- Caffe, P.J., Soler, M.M., Coira, B.L., Onoe, A.T., Cordani, U.G., 2008. The Granada ignimbrite: a compound pyroclastic unit and its relationship with Upper Miocene caldera volcanism in the northern Puna. *Journal of South American Earth Sciences* 25, 464–484.
- Chmielowski, J., Zandt, G., Haberland, C., 1999. The central Andean Altiplano-Puna magma body. *Geophysical Research Letters* 26, 783–786.
- Coira, B., 1973. Resultados preliminares sobre la petrología del ciclo eruptivo ordovícico concomitante con la sedimentación de la Formación Acoite en la zona de Abra Pampa, Provincia de Jujuy, Argentina. *Revista de la Asociación Geológica Argentina* 28, 85–90.
- Coira, B.L., Kay, S.M., Viramonte, J.G., 1993. Upper Cenozoic magmatic evolution of the Argentine Puna - a model for changing subduction geometry. *International Geological Reviews* 35, 677-720.
- Costa, A., Martí, J., 2016. Stress field control during large caldera-forming eruptions. *Frontiers in Earth Science* 4, 92, doi:10.3389/feart.2016.00092.
- de Silva, S.L., 1989. Altiplano–Puna Volcanic Complex of the Central Andes. *Geology* 17, 1102–1106.
- de Silva, S.L., Riggs, N.R., Barth, A.P., 2015. Quickening the pulse: Fractal tempos in continental arc magmatism. *Elements* 11, 113–118.
- Dellino, P., Dioguardi, F., Doronzo, D.M., Mele, D., 2019. The rate of sedimentation from turbulent suspension: an experimental model with application to pyroclastic density currents and discussion on the grain-size dependence of flow runout. *Sedimentology* 66, 129–145.
- Doronzo, D.M., 2012. Two new end members of pyroclastic density currents: forced convection-dominated and inertia-dominated. *Journal of Volcanology and Geothermal Research* 219-220, 87–91.
- Doronzo, D.M., Dellino, P., 2013. Hydraulics of subaqueous ash flows as deduced from their deposits: 2. Water entrainment, sedimentation, and deposition, with implications on pyroclastic density current deposit emplacement. *Journal of Volcanology and Geothermal Research* 258, 176–186.

- Doronzo, D.M., Dellino, P., 2014. Pyroclastic density currents and local topography as seen with the conveyer model. *Journal of Volcanology and Geothermal Research* 278–279, 25–39.
- Doronzo, D.M., Martí, J., Sulpizio, R., Dellino, P., 2012. Aerodynamics of stratovolcanoes during multiphase processes. *Journal of Geophysical Research* 117, B01207, doi: 10.1029/2011JB008769.
- Doronzo, D.M., Martí, J., Dellino, P., Giordano, G., Sulpizio, R., 2016. Dust storms, volcanic ash hurricanes, and turbidity currents: physical similarities and differences with emphasis on flow temperature. *Arabian Journal of Geosciences* 9, 290, doi: 10.1007/s12517-016-2351-8.
- Doronzo, D.M., Dellino, P., Sulpizio, R., Lucchi, F., 2017. Merging field mapping and numerical simulation to interpret the lithofacies variations from unsteady pyroclastic density currents on uneven terrain: the case of La Fossa di Vulcano (Aeolian Islands, Italy). *Journal of Volcanology and Geothermal Research* 330, 36–42.
- Druitt, T.H., 1998. Pyroclastic density currents. In: Gilbert, J.S., Sparks R.S.J. (Eds.), *The physics of explosive eruptions*. Geological Society of London Special Publication 145, pp. 145–182.
- Dufek, J., 2016. The Fluid Mechanics of Pyroclastic Density Currents. *Annual Review of Fluid Mechanics* 48, 459–485.
- Giordano, G., Doronzo, D.M., 2017. Sedimentation and mobility of PDCs: a reappraisal of ignimbrites' aspect ratio. *Scientific Reports* 7, 4444, doi: 10.1038/s41598-017-04880-6.
- Girolami, L., Roche, O., Druitt, T.H., Corpetti, T., 2010. Particle velocity fields and depositional processes in laboratory ash flows, with implications for the sedimentation of dense pyroclastic flows. *Bulletin of Volcanology* 72, 747–759.
- Girolami, L., Druitt, T.H., Roche, O., 2015. Towards a quantitative understanding of pyroclastic flows: Effects of expansion on the dynamics of laboratory fluidized granular flows. *Journal of Volcanology and Geothermal Research* 296, 31–39.
- Grocke, S.B., de Silva, S.L., Wallace, P.J., Cottrell, E., Schmitt, A.K., 2017. Catastrophic Caldera-Forming (CCF) Monotonous Silicic Magma Reservoirs: Constraints from Volatiles in Melt Inclusions from the 3.49 Ma Tara Supereruption, Guacha II Caldera, SW Bolivia. *Journal of Petrology* 58, 227–260.

- Guzmán, S., Petrinovic, I., 2010. The Luingo caldera: the south-easternmost collapse caldera in the Altiplano–Puna plateau, NW Argentina. *Journal of Volcanology and Geothermal Research* 194, 174–188.
- Guzmán, S., Grosse, P., Montero-López, C., Hongn, F., Pilger, R., Petrinovic, I.A., Seggiaro, R., Aramayo, A., 2014. Spatial-temporal distribution of explosive volcanism in the 25–28°S segment of the Andean Central Volcanic zone. *Tectonophysics* 636, 170–189.
- Guzmán, S., Grosse, P., Martí, J., Petrinovic, I.A., Seggiaro, R., 2017. Calderas cenozoicas argentinas de la Zona Volcánica Central de los Andes – procesos eruptivos y dinámica: una revisión. In: Muruaga, C.M., Grosse, P. (Eds.), *Ciencias de la Tierra y Recursos Naturales del NOA. Relatorio del XX Congreso Geológico Argentino*, San Miguel de Tucumán, pp. 518-547.
- Harmon, R.S., Barreiro, B.A., Moorbath, S., Hofes, J., Francis, P.W., Thorpe, R.S., Deruelle, B., McHugh, J., Viglino, J.L., 1984. Regional O-, Sr-, and Pb-isotope relationships in late Cenozoic calcalkaline lavas of the Andean Cordillera. *Journal of the Geological Society of London* 141, 803–822.
- Iriarte, R., 2012. The Cerro Guacha Caldera Complex: An Upper Miocene-Pliocene Polycyclic Volcano-Tectonic Structure in the Altiplano Puna Volcanic Complex of the Central Andes of Bolivia. (Master's thesis). Oregon State University, Corvallis, USA.
- Isacks, B., 1988. Uplift of the Central Andean Plateau and bending of the Bolivian Orocline. *Journal of Geophysical Research* 93, 3211–3231.
- Kay, S.M., Mpodozis, C., Coira, B., 1999. Neogene Magmatism, tectonism, and Mineral Deposits of the Central Andes 22° to 33°S latitude. In: Skinner, B.J. (Ed.); *Geology and Ore Deposits of the Central Andes*. Society of Economic Geologists, Special Publication 7, pp. 27–59.
- Kay, S., Coira, B., Caffè, P., Chen, C.H., 2010. Regional chemical diversity, crustal and mantle sources and evolution of Central Andean Puna plateau ignimbrites. *Journal of Volcanology and Geothermal Research* 198, 81–110.
- Kneller, B.C., Branney, M.J., 1995. Sustained high-density turbidity currents and the deposition of thick massive sands. *Sedimentology* 42, 607–616.

- Lavallée, Y., Wadsworth, F.B., Vasseur, J., Russell, J.K., Andrews, G.D.M., Hess, K., von Aulock, F.W., Kendrick, J.E., Tuffen, H., Biggin, A.J., Dingwell, D.B., 2015. Eruption and emplacement timescales of ignimbrite super-eruptions from thermo-kinetics of glass shards: *Frontiers in Earth Science* 3, doi:10.3389/feart.2015.00002.
- Legros, F., Martí, J., 2001. Formation of inversely graded basal layers in ignimbrites by progressive aggradation. *Journal of Volcanology and Geothermal Research* 111, 25–33.
- Le Pennec, J.-L., Bourdier, J.-L., Froger, J.-L., Temel, A., Camus, G., Gourgaud, A., 1994. Neogene ignimbrites of the Nevşehir Plateau (Central Turkey): stratigraphy, distribution and source constraints. *Journal of Volcanology and Geothermal Research* 63, 59–87.
- Lesti C, Porreca M, Giordano G, Mattei M, Cas RAF, Wright H, Viramonte J., 2011. High temperature emplacement of the Cerro Galán and Toconquis Group ignimbrites (Puna plateau, NW Argentina) determined by TRM analyses. In: Cas RAF, Cashman K (eds) *The Cerro Galán Ignimbrite and Caldera: characteristics and origins of a very large volume ignimbrite and its magma system*. *Bulletin of Volcanology* 73, 1535-1565.
- Lindsay, J.M., de Silva, S., Trumbull, R., Emmermann, R., Wemmer, K., 2001a. La Pacana caldera, N. Chile: a re-evaluation of the stratigraphy and volcanology of one of the world's largest resurgent caldera. *Journal of Volcanology and Geothermal Research* 106, 145–173.
- Lindsay, J.M., Schmitt, A.K., Trumbull, R.B., de Silva, S.L., Siebel, W., Emmermann, R., 2001b. Magmatic evolution of the La Pacana caldera system, central Andes, Chile: Compositional variation of two cogenetic large-volume felsic ignimbrites. *Journal of Petrology* 42, 459–486.
- López, M.E., Guzmán, S., Seggiaro, R., 2016. Estratigrafía de las ignimbritas de la Formación Morro Grande, Puna Norte. VII Congreso Latinoamericano de Sedimentología y XV Reunión Argentina de Sedimentología, La Pampa, Argentina, p. 109.
- Lowe, D.R., 1988. Suspended-load fallout rate as an independent variable in the analysis of current structures sedimentology 35, 765–776.
- Marrett, R., Emerman, S.H., 1992. The relations between faulting and mafic magmatism in the Altiplano-Puna plateau (Central Andes). *Earth and Planetary Science Letters* 112, 53–59.

- Martí, J., Diez-Gil, J.L., Ortiz, R., 1991. Conduction model for the thermal influence of lithic clasts in mixtures of hot gases and ejecta. *Journal of Geophysical Research* 96, 21879–21885.
- Martí, J., Geyer, A., Folch, A., 2009. A genetic classification of collapse calderas based on field studies, and analogue and theoretical modelling. In: Thordarson, T., Self, S., Larsen, G., Rowland, S.K., Hoskuldsson, A. (Eds.), *Studies in Volcanology: The Legacy of George Walker*. Special Publications of IAVCEI, 2. Geological Society, London, pp. 249–266.
- Martí, J., Planagumá, L.I., Geyer, A., Aguirre-Díaz, G., Pedrazzi, D., Bolós, X., 2017. Basaltic ignimbrites in monogenetic volcanism: the example of La Garrotxa volcanic field. *Bulletin of Volcanology* 79, 33, doi:10.1007/s00445-017-1113-0.
- Martí, J., Doronzo, D. M., Pedrazzi, D., Colombo, F., 2019. Topographical controls on small-volume pyroclastic flows. *Sedimentology* 66, 2297–2317.
- McClelland, E., Wilson, C.J.N., Bardot, L., 2004. Paleotemperature determinations for the 1.8 ka Taupo ignimbrite, New Zealand, and implications for the emplacement history of a high velocity pyroclastic flow. *Bulletin of Volcanology* 66, 492-513.
- Michol, K.A., Russell, J.K., Andrews, G.D.M., 2008. Welded block and ash flow deposits from Mount Meager, British Columbia, Canada. *Journal of Volcanology and Geothermal Research* 169, 121-144.
- Mon, R., 1979. Esquema tectónico de los Andes del Norte Argentino. *Revista de la Asociación Geológica Argentina* 34, 70–76.
- Navarrete, C., Butler, K.L., Hurley, M., Marquez, M., 2020. An early Jurassic graben caldera of Chon Aike silicic LIP at the southernmost massif of the world: The Deseado caldera, Patagonia, Argentina. *Journal of South American Earth Sciences* 101, 102626, doi: 10.1016/j.jsames.2020.102626.
- Neri, A., Bevilacqua, A., Esposti Ongaro, T., Isaia, R., Aspinall, W.P., Bisson, M., Flandoli, F., Baxter, P. J., Bertagnini, A., Iannuzzi, E., Orsucci, S., Pistolesi, M., Rosi, M., Vitale, S., 2015. Quantifying volcanic hazard at Campi Flegrei caldera (Italy) with uncertainty assessment: 2.

- Pyroclastic density current invasion maps. *Journal of Geophysical Research Solid Earth* 120, 2330–2349.
- Oncken, O., Hindle, D., Kley, J., Elger, K., Victor, P., Schemmann, K., 2006. Deformation of the Central Andean Upper Plate System-Facts, Fiction, and constraints for plateau models. In: Oncken, O., Chong, G., Franz, G., Giese, P., Götze, H., Ramos, V., Strecker, M., Wigger, P. (Eds.), *The Andes - Active Subduction Orogeny*. Springer, Berlin, pp. 265–283.
- Ort, M., 1993. Eruptive processes and caldera formation in a nested downsag collapse caldera: Cerro Panizos, central Andes Mountains. *Journal of Volcanology and Geothermal Research* 56, 221–252.
- Ort, M.H., Coira, B.L., Mazzoni, M.M., 1996. Generation of a crust-mantle magma mixture: magma sources and contamination at Cerro Panizos, central Andes. *Contributions to Mineralogy and Petrology* 123, 308–322.
- Ort, M.H., de Silva, S.L., Jiménez, N., Jicha, B.R., Singer, B.S., 2013. Correlation of ignimbrites using characteristic remanent magnetization and anisotropy of magnetic susceptibility, Central Andes, Bolivia. *Geochemistry Geophysics Geosystems* 14, 141–157.
- Pacheco-Hoyos, J.G., Aguirre-Díaz, G.J., Dávila-Harris, P., 2018. Boiling-over dense pyroclastic density currents during the formation of the ~ 100 km³ Huichapan ignimbrite in Central Mexico: Stratigraphic and lithofacies analysis. *Journal of Volcanology and Geothermal Research* 349, 268–282.
- Pensa, A., Capra, L., Giordano, G., 2019. Ash clouds temperature estimation. Implication on dilute and concentrated PDCs coupling and topography confinement. *Scientific Reports* 9, 5657, doi:10.1038/s41598-019-42035-x.
- Petrinovic, I.A., Martí, J., Aguirre-Díaz, G.J., Guzmán, S.R., Geyer, A., Salado Paz, N., 2010. The Cerro Aguas Calientes caldera, NW Argentina: an example of a tectonically controlled polygenetic collapse caldera, and its regional significance. *Journal of Volcanology and Geothermal Research* 194, 15–26.

- Platzman, E.S., Sparks, R.S.J., Cooper, F.J., 2020. Fabrics, facies, and flow through a large-volume ignimbrite: Pampa De Oxaya, Chile. *Bulletin of Volcanology* 82, 8, doi:10.1007/s00445-019-1345-2.
- Quane, S.L., Russell, J.K., 2005. Ranking welding intensity in pyroclastic deposits. *Bulletin of Volcanology* 67, 129–143.
- Richards, J.P., Villeneuve, M., 2002. Characteristics of late Cenozoic volcanism along the Archibarca lineament from Cerro Lulluillaco to Corrida de Cori, Northwest Argentina. *Journal of Volcanology and Geothermal Research* 116, 161–200.
- Riller, U., Oncken, O., 2003. Growth of the central Andean plateau by tectonic segmentation is controlled by the gradient in crustal shortening. *Journal of Geology* 111, 367–384.
- Riller, U., Petrinovic, I., Ramelow, J., Strecker, M., Oncken, O., 2001. Late Cenozoic tectonism, caldera and plateau formation in the Central Andes. *Earth Planetary Science Letters* 188, 299–311.
- Robert, G., Andrews, G.D.M., Ye, J., Whittington, A.G., 2013. Rheological controls on the emplacement of extremely high-grade ignimbrites. *Geology* 41, 1031–1034.
- Roche, O., 2012. Depositional processes and gas pore pressure in pyroclastic flows: an experimental perspective. *Bulletin of Volcanology* 74, 1807–1820.
- Roche, O., 2015. Nature and velocity of pyroclastic density currents inferred from models of entrainment of substrate lithic clasts. *Earth Planetary Science Letters* 418, 115–125.
- Roche, O., Phillips, J.C., Kelfoun, K., 2013. Pyroclastic density currents. In: Fagents, S.A., Gregg, T.K.P., Lopes, R.M.C. (Eds.), *Modeling Volcanic Processes: The Physics and Mathematics of Volcanism*. Cambridge University Press, Cambridge, pp. 203–229.
- Roche, O., Buesch, D.C., Valentine, G.A., 2016. Slow-moving and far-travelled dense pyroclastic flows during the Peach Spring super-eruption. *Nature Communications* 7, 10890, doi:10.1038/ncomms10890.
- Rowley, P.J., Roche, O., Druitt, T.H., Cas, R.A.F., 2014 Experimental study of dense pyroclastic density currents using sustained, gas-fluidized granular flows: *Bulletin of Volcanology* 76, 855–868.

- Salisbury, M.J., Jicha, B.R., de Silva, S.L., Singer, B.S., Jiménez, N.C., Ort, M.H., 2011. $^{40}\text{Ar}/^{39}\text{Ar}$ chronostratigraphy of Altiplano-Puna volcanic complex ignimbrites reveals the development of a major magmatic province. *Geological Society of America Bulletin* 123, 821-840.
- Salfity, J.A., 1985. Lineamientos transversales al rumbo Andino en el noroeste Argentino. IV Congreso Geológico Chileno Actas 2, Antofagasta, Chile, pp. 119–137.
- Seggiaro, R.E., 1994. Petrología, geoquímica y mecanismos de erupción del complejo volcánico Coranzulí. (Ph. D. thesis). Universidad Nacional de Salta, Argentina.
- Seggiaro, R., Aniel, B., 1989. Los ciclos piroclásticos cenozoicos del área Tiomayo Coranzulí Jujuy Argentina. *Revista de la Asociación Geológica Argentina* 44, 394–401.
- Seggiaro, R., Gorustovich, S., Martí, J., 1987. Las ignimbritas del Complejo Volcánico Coranzulí (Puna Argentina-Andes Centrales). *Estudios Geológicos* 43, 345–358.
- Seggiaro, R., Guzmán, S., Martí, J., Montero-López, C., López, E., 2014. Stratigraphy of the Coranzulí caldera. In: Rocha, R., Pais, J., Kullberg, J. C., Finney, S. (Eds.), *Strati 2013: First International Congress on Stratigraphy. At the cutting edge of stratigraphy*. Springer Geology, Cham, pp. 1269–1273.
- Seggiaro, R., Guzmán, S., Martí, J., 2019. Dynamics of caldera collapse during the Coranzulí eruption (6.6 Ma) (Central Andes, Argentina). *Journal of Volcanology and Geothermal Research* 347, 1–12.
- Self, S., 2006. The effects and consequences of very large explosive volcanic eruptions: Philosophical Transactions of the Royal Society A 364, 2073–2097.
- Smith, R.L., 1960. Zones and zonal variations in welded ash-flows, US Geological Survey Professional paper 354-F, Washington, pp. 149-159.
- Soler, M.M., Caffè, P.J., Coira, B.L., Onoe, A.T., Kay, S.M., 2007. Geology of the Vilama caldera: a new interpretation of a large-scale explosive event in the Central Andean plateau during the Upper Miocene. *Journal of Volcanology and Geothermal Research* 164, 23–53.
- Sparks, R.S.J., Wilson, L., 1976. A model for the formation of ignimbrite by gravitational column collapse. *Journal of the Geological Society of London* 132, 441–451.
- Sparks, R.S.J., Self, S., Walker, G.P.L., 1973. Products of ignimbrite eruption. *Geology* 1, 115–118.

- Sparks, R.S.J., Wilson, L., Hulme, G., 1978. Theoretical modeling of the generation, movement, and emplacement of pyroclastic flows by column collapse. *Journal of Geophysical Research Solid Earth* 83 (B4), 1727–1739.
- Sparks, R., Francis, P., Hamer, R., Pankhurst, R., O'Callaghan, L., Thorpe, R. S., Page, R., 1985. Ignimbrites of the Cerro Galán caldera, NW Argentina. *Journal of Volcanology and Geothermal Research* 24, 205–24.
- Stern, C.R., 2004. Active Andean volcanism: its geologic and tectonic setting. *Revista Geológica de Chile* 31, 161–206.
- Sulpizio, R., Dellino, P., 2008. Sedimentology, depositional mechanisms and pulsating behavior of pyroclastic density currents. In: Martí, J., Gottsman, J. (Eds.), *Caldera volcanism: analysis, modelling and response*. *Developments in Volcanology*, 10. Elsevier, Amsterdam, pp. 57–96.
- Sulpizio, R., Mele, D., Dellino, P., La Volpe, L., 2007. Deposits and physical properties of pyroclastic density currents during complex Subplinian eruptions: the AD 472 (Pollena) eruption of Somma-Vesuvius, Italy. *Sedimentology* 54, 607–635.
- Sulpizio, R., Dellino, P., Doronzo, D.M., Sarocchi, D., 2014. Pyroclastic density currents: state of the art and perspectives. *Journal of Volcanology and Geothermal Research* 283, 36–65.
- Sulpizio, R., Castioni, D., Rodriguez-Sedano, L.A., Sarocchi, D., Lucchi, F., 2016. The influence of slope-angle ratio on the dynamics of granular flows: insights from laboratory experiments. *Bulletin of Volcanology* 78, 77, doi:10.1007/s00445-016-1069-5.
- Sweeney, M. R., Valentine, G. A., 2017. Impact zone dynamics of dilute mono- and polydisperse jets and their implications for initial conditions of pyroclastic density currents. *Physics of Fluids* 29, 093304, doi:10.1063/1/5004197.
- Tibaldi, A., Bonali, F., Corazzato, C., 2017. Structural control on volcanoes and magma paths from local to orogeny-scale: The Central Andes case. *Tectonophysics* 699, 14–41.
- Troise, M., Giordano, G., Cifelli, F., Winkler, A., Mattei, M., 2017. Forced transport of thermal energy in magmatic and phreatomagmatic large volume ignimbrites: paleomagnetic evidence from the Colli Albani volcano, Italy. *Earth and Planetary Science Letters* 478, 179–191.

- Trumbull, R.B., Riller, U., Oncken, O., Scheuber, E., Munier, K., Hongn, F., 2006. The time–space distribution of Cenozoic arc volcanism in the Central Andes: a new data compilation and some tectonic considerations. In: Oncken, O., Chong, G., Franz, G., Giese, P., Götze, J., Ramos, V., Strecker, M., Wigger, P. (Eds.), *The Andes–Active Subduction Orogeny*. *Frontiers in Earth Science Series 1*. Springer-Verlag, Berlin, pp. 29–43.
- Walker, G.P.L., 1972. Crystal concentration in ignimbrites. *Contributions to Mineralogy and Petrology* 36, 135–146.
- Willcock, M.A.W., Cas, R.A.F., Giordano, G., Morelli, C., 2013. The eruption, pyroclastic flow behaviour, and caldera in-filling processes of the extremely large volume ($> 1290 \text{ km}^3$), intra- to extra-caldera, Permian Ora (Ignimbrite) Formation, Southern Alps, Italy. *Journal of Volcanology and Geothermal Research* 265, 102–126.
- Wilson, C.J.N., Hildreth, W., 2003. Assembling an ignimbrite: mechanical and thermal building blocks in the Bishop Tuff, California. *Journal of Geology* 111, 653–670.

Figure captions:

Fig. 1. Calderas and caldera-related ignimbrites of the Altiplano-Puna Volcanic Complex, modified from Petrinovic et al. (2010) and Guzmán et al. (2017).

Fig. 2. Ignimbrite units from the Coranzulí caldera shown in a Shuttle Radar Topographic Mission Digital Elevation Model. Black circles with numbers refer to the 20 new stratigraphic logs shown in Fig. 3 and Table 1.

Fig. 3. Stratigraphic logs in (a) northern, (b) eastern, (c) northwestern and (d) southern directions from the caldera.

Fig. 4. Pre-caldera block and ash flow deposit and ignimbrite unit 1. (a) General view with monolithologic massive breccia, in which lithics consist only of dacitic lavas, fine-grained cross-stratified facies, massive lithic breccia facies rich in dacitic lithic fragments with some Ordovician

metapelites and quartzites, followed by a massive ignimbrite facies, (b) detail of monolithologic massive breccia formed by dacitic lithics, (c) detail of fine-grained cross-stratified facies, (d) lithic-rich lenses within the fine-grained cross-stratified facies, (e) detail of massive lithic breccia facies rich in dacitic fragments with subordinated Ordovician metapelites and quartzites.

Fig. 5. (a) Detail of black fiammes, (b) detail of a pink fiamme, (c) detail of crystal-rich pumices in non-welded facies; a dense juvenile grey fragment is visible in the upper right, (d) detail of grey fiammes in welded facies.

Fig. 6. (a, b) Ignimbrite unit 2: (a) Lenticular lithic-rich facies interlayered within the massive ignimbrite, (b) detail of lenticular lithic-rich facies; note the subangular fragments; (c, d) Ignimbrite unit 3: (c) massive lithic breccia facies, (d) general view of the massive ignimbrite facies with columnar jointing at medial facies.

Fig. 7. Ignimbrite unit 4. (a) Detail of fine-grained cross-stratified facies, (b) detail of fine-grained planar-stratified facies with levels of concentration of pumices, (c) intercalated sets of fine-grained cross-stratified and massive ignimbrite facies, (d) detail of pumice-rich facies with dark colours due to preferential alteration, (e) columnar jointing in welded ignimbrites near the southern rim of the caldera; note the deformation in the upper portions, (f) pumice-rich massive ignimbrite facies with blocks of dacitic ignimbrite indicated by an arrow, (g) detail of pumice-rich massive ignimbrite, (h) massive lithic breccia facies with blocks of dacitic ignimbrite.

Fig. 8. Sedimentation rate as a function of the T_{dep}/T_g ratio calculated for different shear zone thicknesses (1–2 m) and for different large eruption durations (5–50 h). The grey area represents the thermo-mechanical conditions in which ductile deformation is possible within the aggrading deposit.

Fig. 9. Schematic reconstruction of facies architecture of the Coranzulí ignimbrites derived from facies relations from stratigraphic logs of this work and from Seggiaro et al. (2019). General views in (a)

northern, (b) eastern, (c) north-western and (d) southern directions from the caldera. These cartoons are not to scale.

Table captions:

Table 1. Field data corresponding to the local deposit thickness, h , and the application of the model to calculate ranges of the accumulation rate, A_r , emplacement timescale, t , and accumulation velocity, h/t ; * no log is available for this point, only its thickness at the locations shown in Fig. 2.

Journal Pre-proof

<i>Profile</i> (Figs.2, 3)	<i>h</i> [m]	<i>A</i> , min-max [kg/m ² s]	<i>t</i> min-max [min]	<i>h/t</i> min-max [mm/s]
21*	12	0.6 - 11.2	25.0 - 500.0	0.4 - 8.0
17	23	2.1 - 41.1	13.0 - 260.9	1.5 - 29.4
18	80	24.9 - 497.8	3.7 - 75.0	17.8 - 355.6
20	16	1.0 - 19.9	18.7 - 375.0	0.7 - 14.2
7	6	0.1 - 2.8	50.0 - 1000.0	0.1 - 2.0
8	50	9.7 - 194.4	6.0 - 120.0	6.9 - 138.9
2	85	28.1 - 561.9	3.5 - 70.6	20.1 - 401.4
5	200	155.5 - 3111.1	1.5 - 30.0	111.1 - 2222.2
12	87	29.4 - 588.7	3.4 - 69.0	21.0 - 420.5
14	50	9.7 - 194.4	6.0 - 120.0	6.9 - 138.9
6	51	10.1 - 202.3	5.9 - 117.6	7.2 - 144.5
10	12	0.6 - 11.2	25.0 - 500.0	0.4 - 8.0
4	10	0.4 - 7.8	30.0 - 600.0	0.3 - 5.6
9	141	77.3 - 1546.3	2.1 - 42.5	55.2 - 1104.5

Table 1

Declaration of competing interest

The authors declare that they have no known competing financial interests or personal relationships that could have appeared to influence the work reported in this paper.

Journal Pre-proof

Highlights

- Coranzulí caldera generated four ignimbrite units at 6.6 Ma
- A theoretical model of emplacement dynamics was developed
- Dense PDCs were subject to rapid *en masse* emplacement
- Emplacement was influenced by paleotopography only locally
- PDCs travelled at relatively low velocities (less than tens of m/s)

Journal Pre-proof

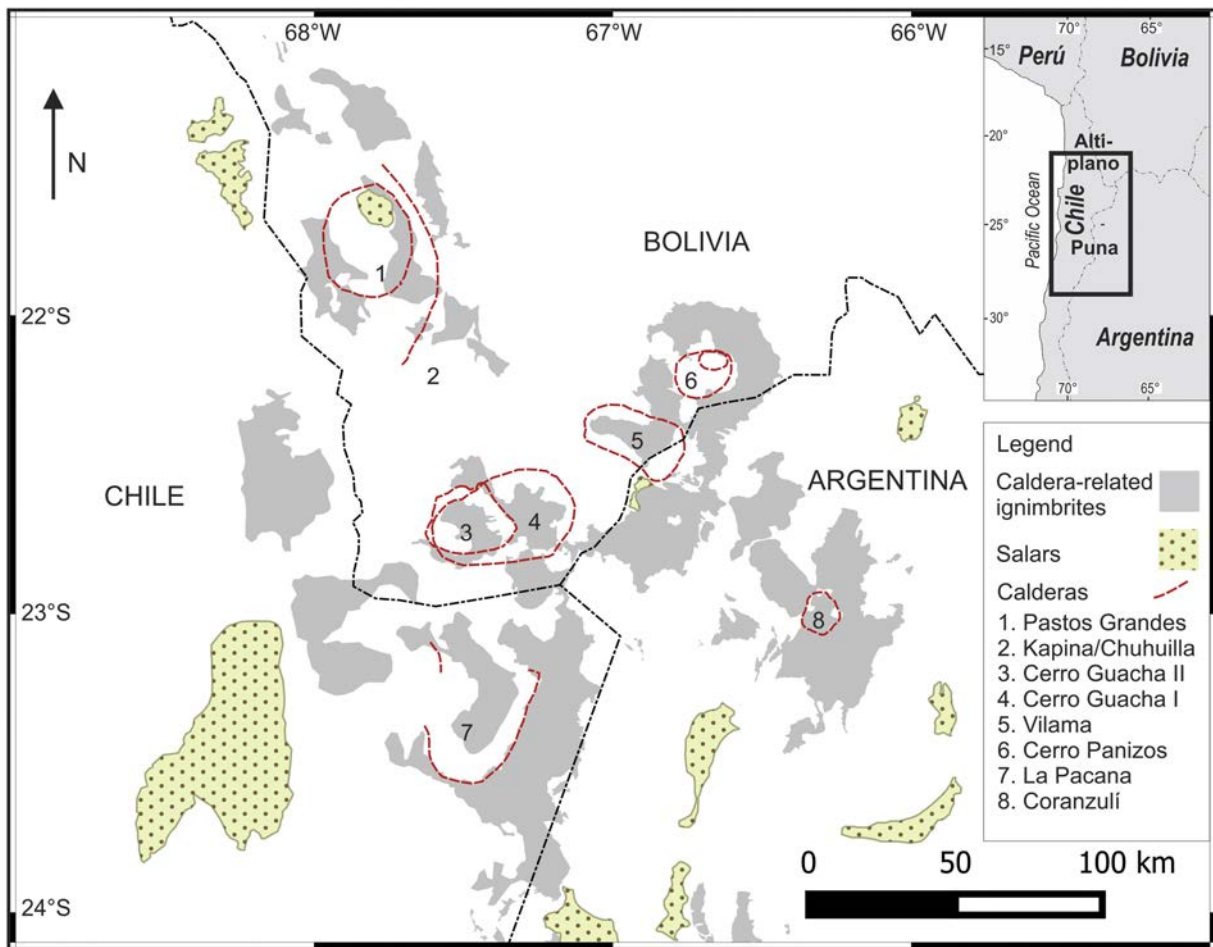


Figure 1

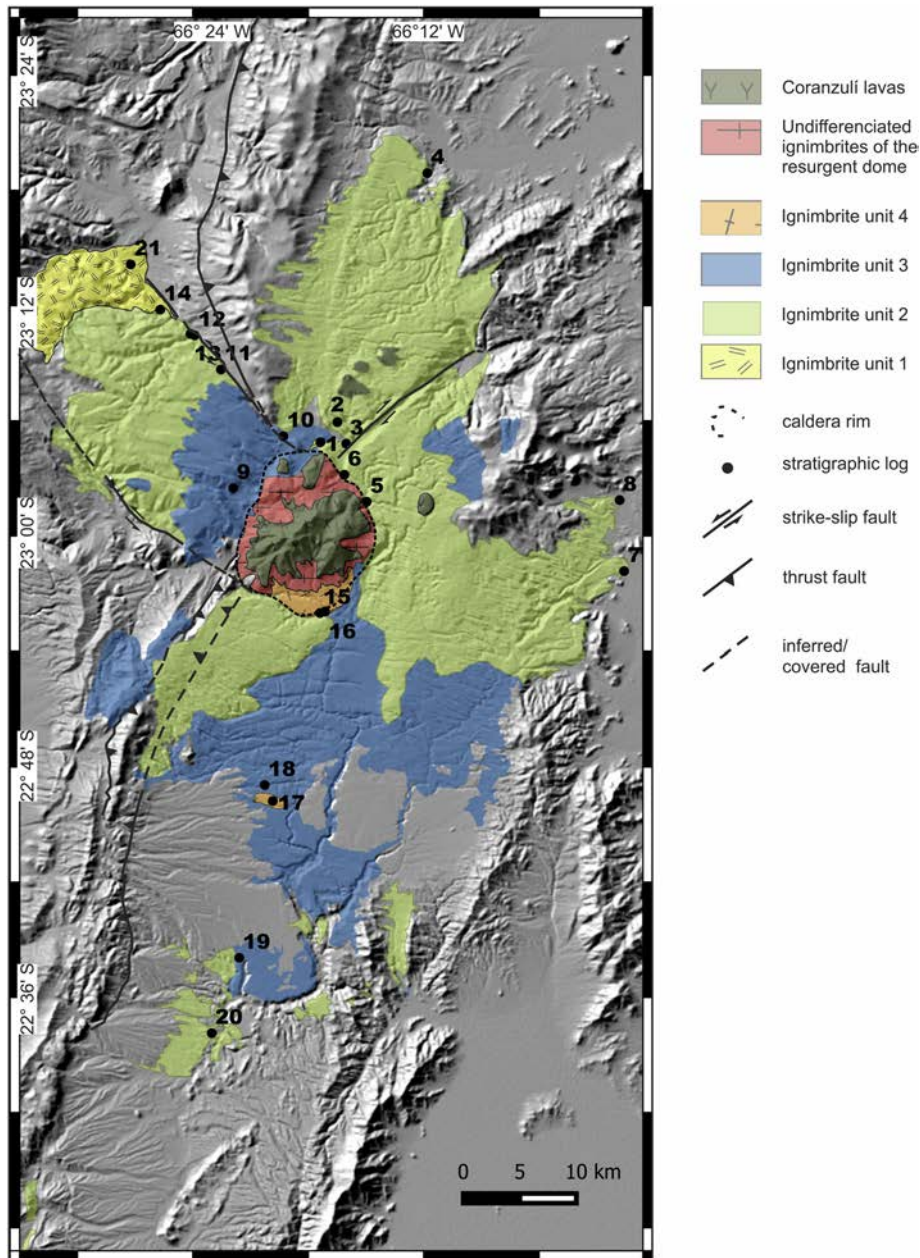


Figure 2

(a)

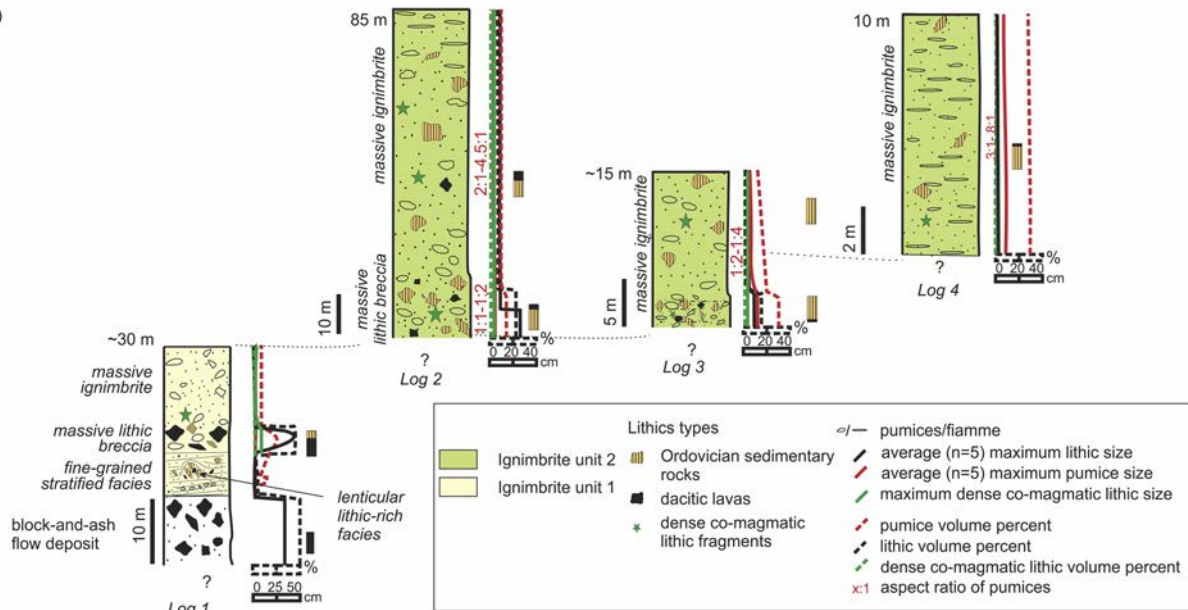


Figure 3a

Profiles to the east of Coranzuli caldera

(b) 200 m

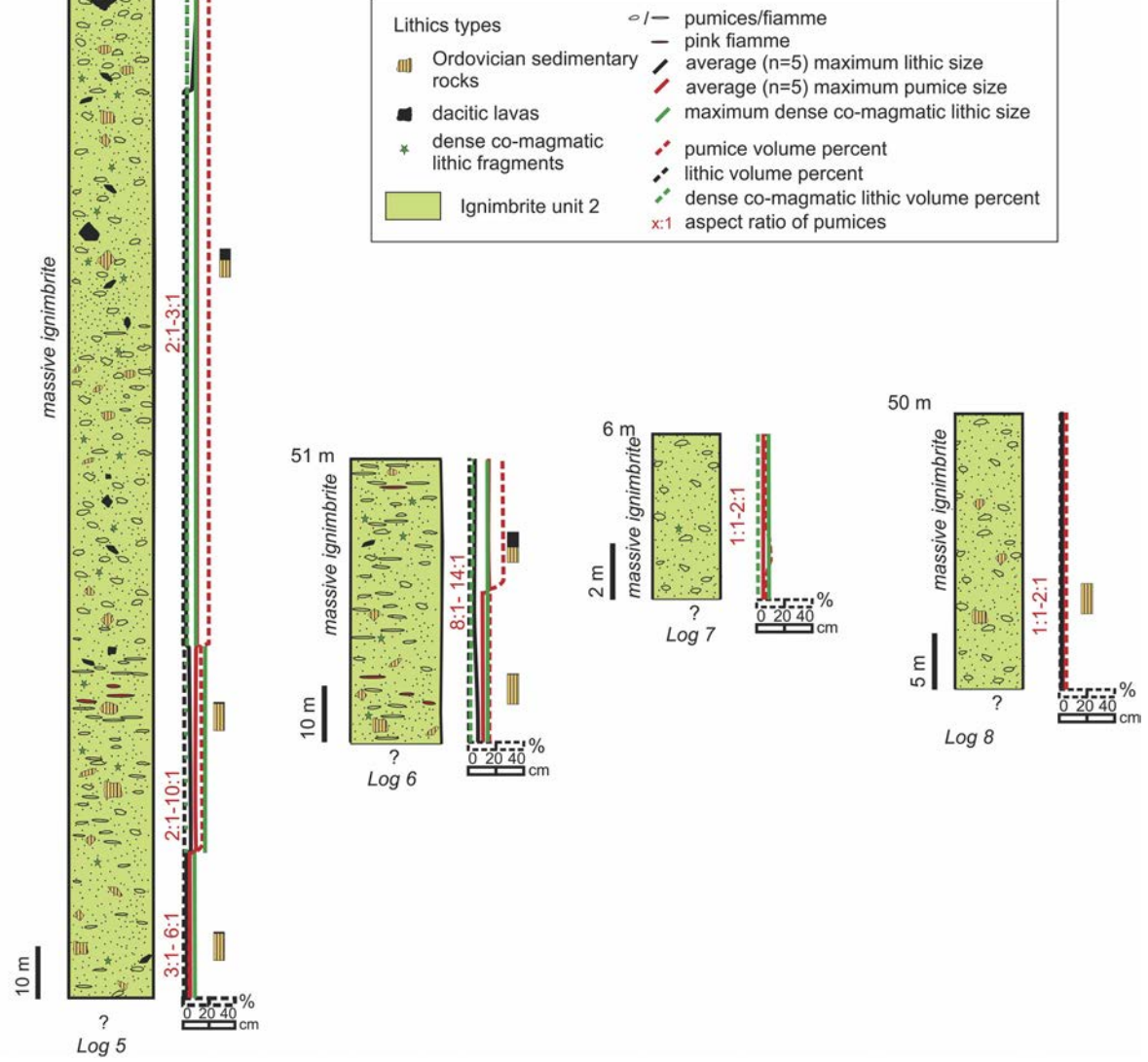


Figure 3b

Profiles to the NW of the caldera

(c)

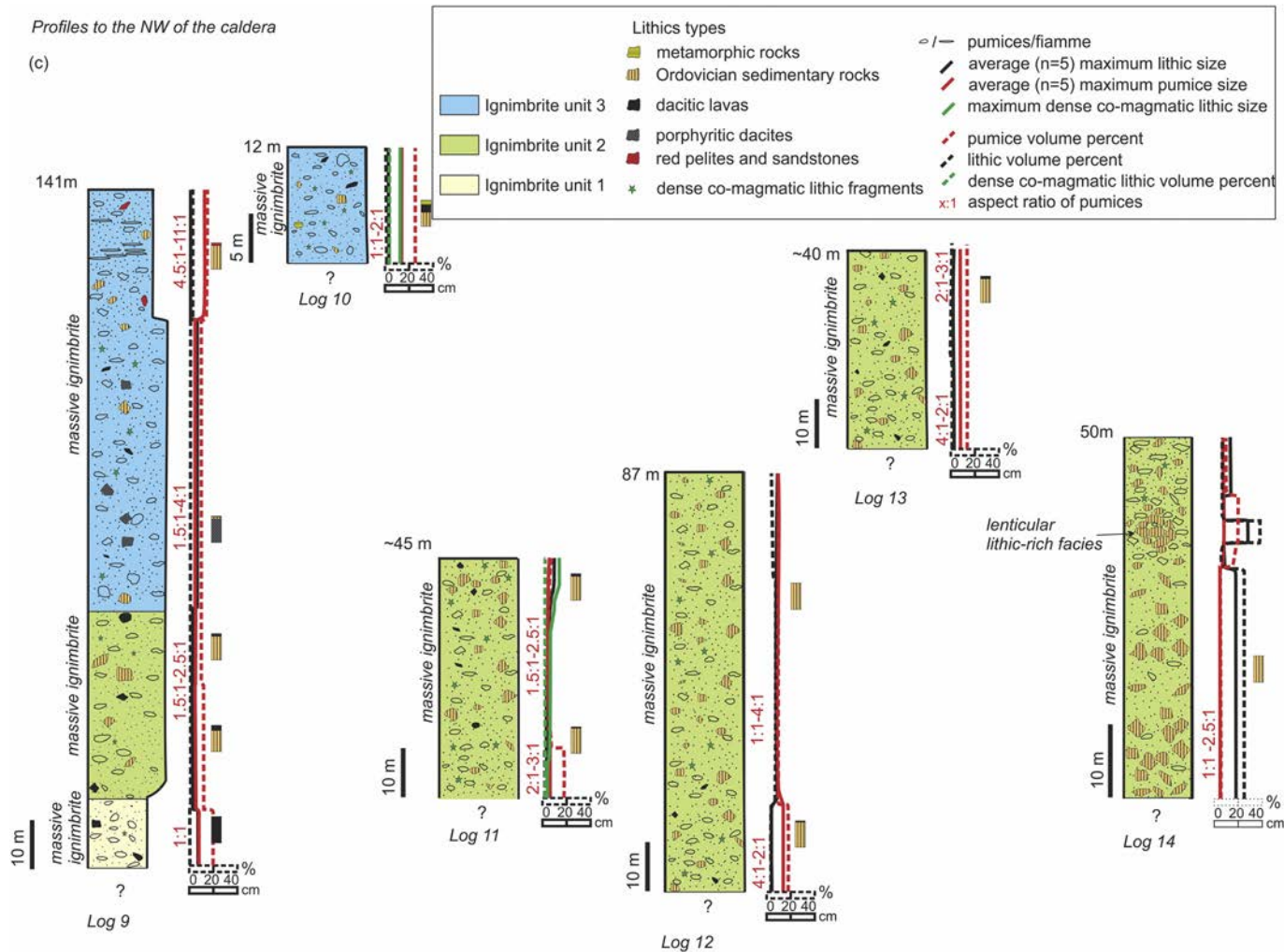


Figure 3c

(d)

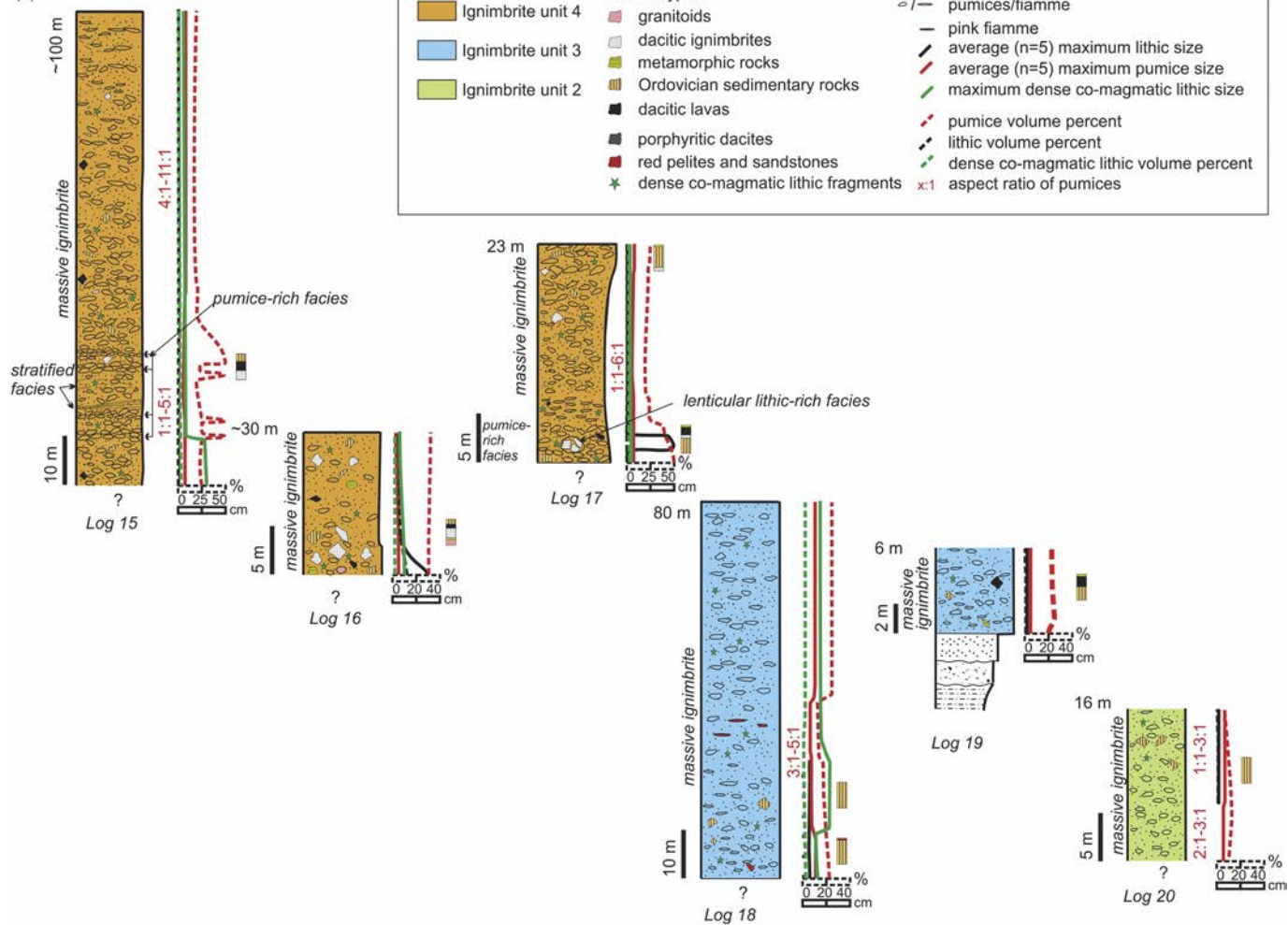


Figure 3d



Figure 4



Figure 5



Figure 6



a



b



c



d



e



f



g



h

Figure 7

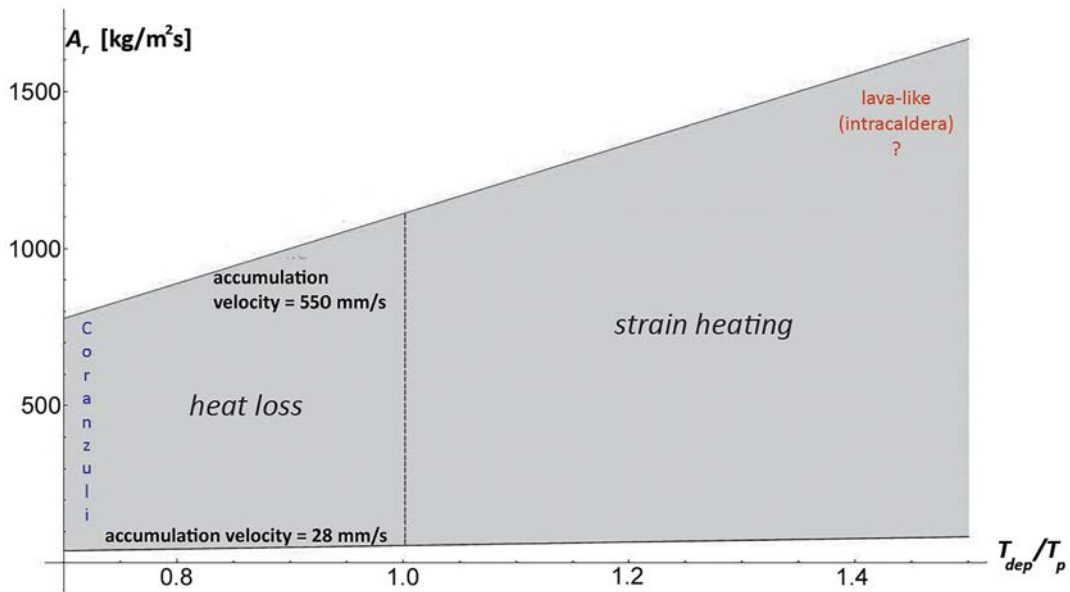


Figure 8

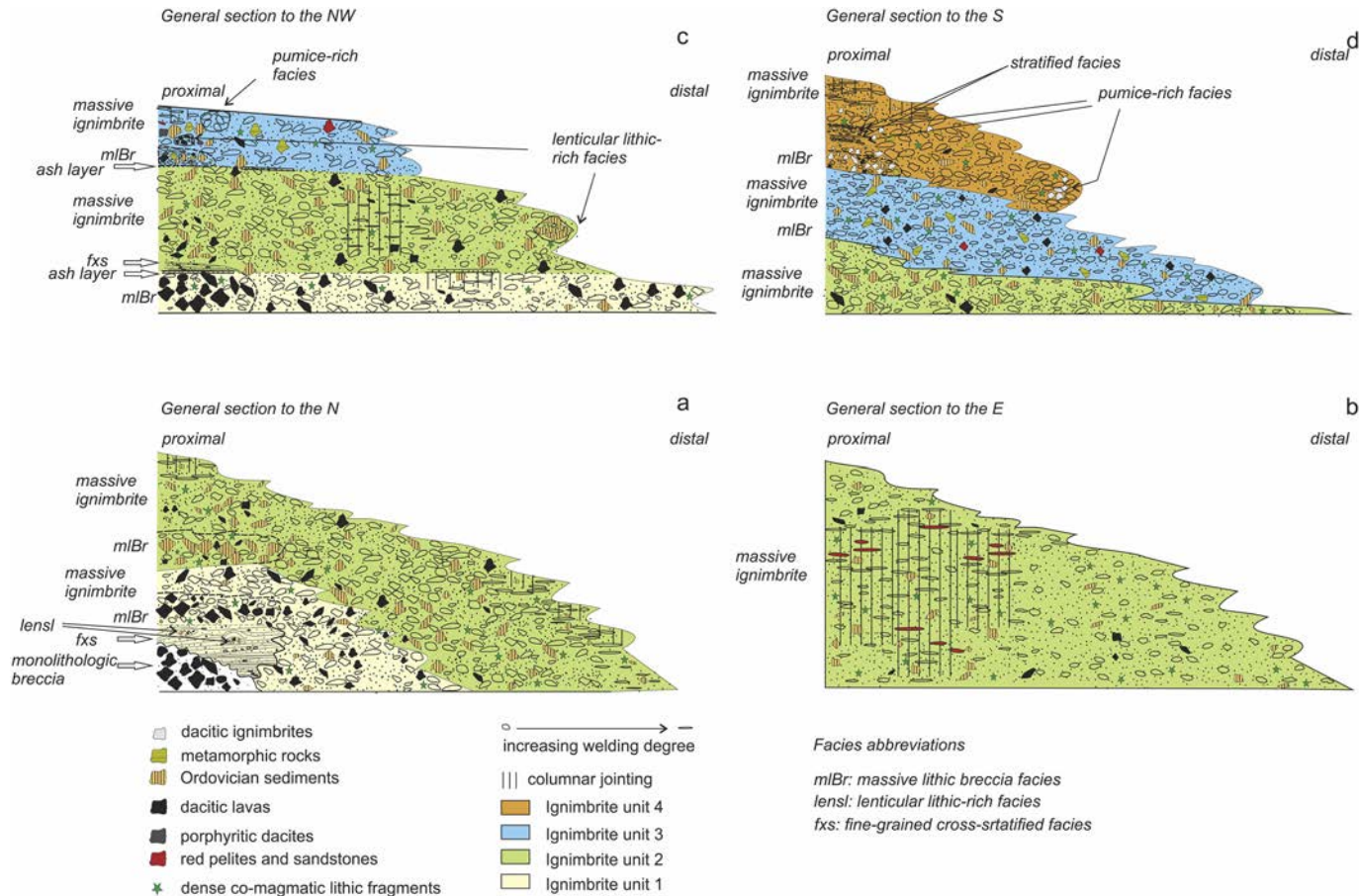


Figure 9